

# The Environments of Luminous Fast Blue Optical Transients: Evidence for a Compact Object and Wolf-Rayet Star Merger Origin

ANYA E. NUGENT <sup>1</sup>, V. ASHLEY VILLAR <sup>1,2</sup>, BRIAN D. METZGER <sup>3,4</sup>, CHRISTOPHER L. FRYER <sup>5</sup>, ERIC BURNS <sup>6</sup>,  
ALEXA C. GORDON <sup>7</sup> AND DANIELLE FROSTIG <sup>1</sup>

<sup>1</sup>Center for Astrophysics | Harvard & Smithsonian, 60 Garden St. Cambridge, MA 02138, USA

<sup>2</sup>The NSF AI Institute for Artificial Intelligence and Fundamental Interactions

<sup>3</sup>Center for Computational Astrophysics, Flatiron Institute, 162 W. 5th Avenue, New York, NY 10011, USA

<sup>4</sup>Department of Physics and Columbia Astrophysics Laboratory, Columbia University, New York, NY 10027, USA

<sup>5</sup>Center for Nonlinear Studies, Los Alamos National Laboratory, Los Alamos, NM 87545 USA

<sup>6</sup>Department of Physics & Astronomy, Louisiana State University, Baton Rouge, LA 70803, USA

<sup>7</sup>Center for Interdisciplinary Exploration and Research in Astrophysics (CIERA) and Department of Physics and Astronomy, Northwestern University, Evanston, IL 60208, USA

## ABSTRACT

We present a comprehensive analysis of the host galaxies of 11 luminous fast blue optical transients (LFBOTs). We model new and archival host photometry and spectroscopy with *Prospector*. We determine that all LFBOT hosts are actively star-forming with recent bursts of star formation and have a median stellar mass of  $\log(M_*/M_\odot) = 9.61^{+0.74}_{-1.61}$ , present-day star formation rate  $\text{SFR} = 0.95^{+18.37}_{-0.91} M_\odot \text{ yr}^{-1}$ , and gas-phase oxygen abundance metallicity  $12 + \log(\text{O}/\text{H}) = 8.71^{+0.17}_{-0.40}$ . To contextualize these results, we compare them to the host properties of Hydrogen-poor superluminous supernovae (SLSNe-I), several core-collapse supernova subtypes (CCSN; SNe Ibc, II, and Ibn) and long gamma-ray bursts (LGRBs). We find that LFBOT hosts are more star-forming than CCSN hosts, but less star-forming than SLSN-I hosts. We further show that LFBOT hosts are more metal-poor than SN Ibc and II hosts, but more metal-rich than SLSN-I and LGRB hosts. Finally, we find that, similar to SLSNe-I and unlike CCSNe and LGRBs, a large fraction ( $> 30\%$ ) of LFBOTs occur in their hosts’ faintest pixel or outside their host galaxy’s light. Our results indicate that LFBOTs have massive stellar origin that do not trace active star-forming regions within their hosts and have a weaker metallicity-dependence than other extreme transients. For these reasons, we favor a compact-object and Wolf-Rayet star merger progenitor scenario. Future discoveries of LFBOTs with the Rubin observatory will help to increase their sample size and place firmer constraints on their environments and progenitors.

*Keywords:* transients, supernovae, galaxies, surveys, stellar populations

## 1. INTRODUCTION

Luminous Fast Blue Optical Transients (LFBOTs), or “cow-like” events after the prototypical member AT2018cow (Prentice et al. 2018; Ho et al. 2019; Margutti et al. 2019; Perley et al. 2019), represent a unique class of extreme astrophysical transient phenomena. LFBOTs are characterized by their rapid lightcurve evolution, reaching peak brightness in  $\lesssim 1$  week and de-

caying to half-peak brightness in a similar time, and high peak optical luminosities ( $L_{\text{peak}} > 10^{43} \text{ erg s}^{-1}$ ) that rival those of superluminous supernovae (SLSNe). Importantly, their lightcurves cannot be explained by the radioactive decay of  $^{56}\text{Ni}$ , thereby distinguishing LFBOTs from “normal” supernovae (SNe) and core-collapse (CC) events (Perley et al. 2019). LFBOT spectra are dominated by a hot, blue, featureless continuum (blackbody temperatures  $> 10^4 \text{ K}$ ) for weeks after they reach peak brightness, hinting that they are powered by a central heating source. The luminous and variable X-ray emission observed for several events further corroborates this

idea and signifies that the central engine is likely a compact object (Margutti et al. 2019; Coppejans et al. 2020; Perley et al. 2021; Ho et al. 2022; Yao et al. 2022; Ho et al. 2023a; Chrimes et al. 2024a; Nayana et al. 2025; Omand et al. 2026). In addition, a handful of LFBOTs appear to have bright radio and millimeter emission, deduced to come from a dense, extended circumstellar medium (CSM) surrounding the central engine (Ho et al. 2019, 2020, 2022; Margutti et al. 2019; Coppejans et al. 2020; Bright et al. 2022; Yao et al. 2022; Chrimes et al. 2024a,b; Nayana et al. 2025; Sevilla et al. 2026).

While there are now 11 *bona-fide* events that comprise the LFBOT class, the nature of their progenitor and central engine still remains highly uncertain. Given that LFBOTs are intrinsically rare transients ( $< 1\%$  the CCSN volumetric rate; Coppejans et al. 2020; Ho et al. 2023b), they likely have unusual astrophysical origins. For example, it has been theorized that LFBOTs could represent rare end-states to massive star evolution, such as failed SNe that create accreting black holes (BH; Margutti et al. 2019; Perley et al. 2019; Quataert et al. 2019; Antoni & Quataert 2022), pulsational-pair instability SNe (PPISNe; Leung et al. 2020), or magnetar-powered SNe (Prentice et al. 2018; Vurm & Metzger 2021). These theories, in particular, directly connect LFBOTs to other transient phenomena from stellar deaths, including: CCSNe, long gamma-ray bursts (LGRBs; arise from collapsars), and hydrogen-poor SLSNe (SLSNe-I; thought to originate from magnetar-powered core-collapse events). On the other hand, Metzger (2022) and Klencki & Metzger (2025) hypothesize that LFBOTs (and possibly Type Ibn and Icn SNe) originate from mergers of stellar-mass BHs or neutron stars (NSs) with Wolf-Rayet (WR) stars. Given the observational similarities of LFBOTs to TDEs of supermassive BHs (SMBH), it has also been proposed they may derive from TDEs of intermediate-mass BHs (IMBHs; Kuin et al. 2019; Perley et al. 2019; Ho et al. 2023a) or stellar-mass BHs or NSs (Tsunai & Lu 2025). Finally, several studies have debated whether LFBOTs simply represent shock interactions with dense CSM material (Margalit et al. 2022; Pellegrino et al. 2022; Gutiérrez et al. 2024; Khatami & Kasen 2024; Govreen-Segal et al. 2026).

The lack of consensus on LFBOT origins from their observed characteristics motivates consideration of properties independent of their transient emission to place meaningful constraints on their progenitors. Indeed, their host galaxies may be vital in this effort, as the connection of transients to their environments gives critical insight into their progenitor formation pathways and timescales (c.f., Prieto et al. 2008; Svensson et al.

2010; Anderson & James 2009; Arcavi et al. 2010; Li et al. 2011; Schulze et al. 2021; Taggart & Perley 2021; Qin & Zabludoff 2024; Nugent et al. 2026). Several studies on individual (or a smaller subset of) LFBOTs have found that they typically occur in actively star-forming, low-mass galaxies with low metallicities (Perley et al. 2019; Coppejans et al. 2020; Ho et al. 2020; Yao et al. 2022; Perley et al. 2019; Sevilla et al. 2026). At face value, the presence of LFBOTs in this particular environment may hint that they originate from young massive star progenitors, as is the case for other transient populations observed in similar hosts, like LGRBs and SLSNe-I (Svensson et al. 2010; Perley & Perley 2013; Chen et al. 2013; Lunnan et al. 2014, 2015; Angus et al. 2016; Perley et al. 2016; Schulze et al. 2018, 2021; Taggart & Perley 2021). This was further inferred in Sun et al. (2023), where they determined that AT2018cow was spatially coincident with a star-bursting region within its host, where it is presumed that a large, massive star population may exist. On the contrary, Chrimes et al. (2024b) found that LFBOT AT2023fhn was  $\approx 17$  kpc from its host galaxy’s center, far removed from any star-formation. This offset is quite large in comparison to those observed for CCSNe, LGRBs, and SLSNe-I, thereby challenging progenitor scenarios tied to young stellar populations. Thus, a uniform analysis of LFBOT environments is critical to characterize their host properties, galactocentric offsets, and connection to recent star formation, which, ultimately, may clarify the nature of their progenitors.

Here, we present a uniform analysis of the host galaxy and environmental properties of 11 LFBOTs: AT2018cow (Prentice et al. 2018; Ho et al. 2019; Margutti et al. 2019; Perley et al. 2019), CSS161010 (Coppejans et al. 2020; Gutiérrez et al. 2024), ZTF18abvkw (Ho et al. 2020), AT2020mrf (Yao et al. 2022), AT2020xnd (Perley et al. 2021; Bright et al. 2022; Ho et al. 2022), AT2022tsd (Ho et al. 2023a), AT2023fhn (Chrimes et al. 2024a,b; Sevilla et al. 2026), AT2023hkw (Sevilla et al. 2026), AT2023vth (Sevilla et al. 2026), AT2024qfm (Sevilla et al. 2026), and AT2024wpp (Pursiainen et al. 2025; LeBaron et al. 2026; Nayana et al. 2025; Omand et al. 2026; Perley et al. 2026). This represents the largest sample of LFBOT host galaxy analysis thus far in the literature. We take advantage of previously published host associations in the aforementioned literature to conduct our environmental analysis. We note that there are two other claimed LFBOTs that we do not include in this study: AT2022abfc and AT2024aehp (Sevilla et al. 2026). We exclude AT2022abfc as there is a lack of optical lightcurve information that hinders our confidence in its characteriza-

tion as an LFBOT, and we exclude AT2024aehp given that its optical lightcurve at late times deviates from other well-studied LFBOTs. In Section 2, we detail photometric and spectroscopic observations of the host galaxies. We discuss our host galaxy stellar population modeling techniques in Section 3. We present our main findings on LFBOT host properties and compare them to host properties of other well-studied transient populations in Section 4. We furthermore perform an analysis on the LFBOT galactocentric offsets and fractional fluxes in Section 5. Finally, we postulate on the LFBOT progenitor in Section 6 and discuss our main conclusions in Section 7.

Unless otherwise stated, all observations are reported in the AB magnitude system and have been corrected for Galactic extinction in the direction of the object of interest using the Schlafly & Finkbeiner (2011) extinction maps. We employ a standard WMAP9 cosmology of  $H_0 = 69.6 \text{ km s}^{-1} \text{ Mpc}^{-1}$ ,  $\Omega_{\text{m}} = 0.286$ ,  $\Omega_{\text{vac}} = 0.714$  (Hinshaw et al. 2013; Bennett et al. 2014).

## 2. OBSERVATIONS

### 2.1. Photometry

We collect photometric observations of LFBOT host galaxies using a combination of previously published photometry, data from our own observing programs, and publicly available data from archival surveys. We collect available host galaxy photometry for AT2018cow, ZTF18abvkw (u-band), AT2020mrf, and AT2020xnd from Perley et al. (2019), Ho et al. (2020), Yao et al. (2022), and Perley et al. (2021), respectively. For the hosts of AT2020xnd (r-band), AT2022tsd (r and z-band), and AT2024wpp (giz-bands), we obtain  $15 \times 120$  sec exposures ( $20 \times 90$  sec for the z-band observations) with the 6.5-m MMT Observatory’s Binospec optical imager and spectrograph (PI: Nugent). We furthermore obtain  $7 \times 200$  sec exposures in V-band for the host of AT2023fhn and  $9 \times 200$  sec exposures in G-band for the host of AT2022tsd with the 10-m Keck Observatory’s Low Resolution Imaging Spectrometer (LRIS; PI: Gordon). For the hosts of AT2024qfm and AT2024wpp, we collect near-IR *YJHK* imaging (30 min total exposure time) with the MMT’s MMT and Magellan Infrared Spectrograph (MMIRS; PI: Frostig).

We reduce all photometric images from our programs using POTPyRI<sup>1</sup> (Pipeline for Optical/infrared Telescopes in Python for Reducing Images; Paterson 2021), which performs bias subtraction, flat fielding, astrometry (via Astrometry.net; Lang et al. 2010), image

alignment and stacking, PSF photometry, and flux calibration. We perform aperture photometry on the hosts using SEP (Barbary 2016), a Python-based version of Source Extractor (Bertin & Arnouts 1996). Within SEP, we measure Kron radii of the hosts and extract a photometric measurement and uncertainty within these radii, using their standard `sep.sum_ellipse` routine.

For the hosts of CSS161010, ZTF18abvkw, AT2022tsd, AT2023fhn, A2023hkw, AT2023vth, AT2024qfm, and AT2024wpp, we use FrankenBlast (Nugent et al. 2026), a customized version of the Blast web-application (Jones et al. 2024), to obtain additional photometry of the hosts from publicly archival surveys. FrankenBlast collects images of the hosts from the *Galaxy Evolution Explorer* (GALEX; Bouquin et al. 2018), the Panoramic Survey Telescope and Rapid Response System (Pan-STARRS; Chambers et al. 2016), the Dark Energy Camera Legacy Survey (DECaLS) Data Release 10 (Dey et al. 2019), the *Two Micron All-Sky Survey* (2MASS; Skrutskie et al. 2006), and the *Wide-field Infrared Survey Explorer* (WISE; Wright et al. 2010). In each of the obtained images, FrankenBlast constructs an elliptical aperture around the host and extracts a flux measurement and uncertainty via Astropy photutils (Bradley et al. 2025). We refer the readers to Nugent et al. (2026) for more details on their photometric technique. We list all host galaxy photometric observations used in the stellar population modeling fits (Section 3) and magnitudes (not corrected for Galactic extinction) in Table A1.

### 2.2. Spectroscopy

We supplement our photometric observations with host galaxy spectra from both our own programs and archival data that were previously-published. We obtain MMT/Binospec spectra (PI: Nugent) for the hosts of AT2018cow, AT2020xnd, AT2020tsd, AT2023fhn, AT2023hkw, AT2024qfm, and AT2024wpp. We further collect archival spectroscopic observations from Keck/LRIS for the hosts of CSS161010, ZTF18abvkw, and AT2020mrf, which were originally published in Coppejans et al. (2020), Ho et al. (2020), and Yao et al. (2022), respectively. We list all spectroscopic observations and exposure times in Table A2.

We use PyPeIt (Prochaska et al. 2020) to reduce the MMT/Binospec and Keck/LRIS observations and extract the 1D spectra. We do not re-reduce the host spectrum of ZTF18abvkw as Ho et al. (2020) published a flux-calibrated 1D host spectrum available for download. We employ the standard PyPeIt pipeline to perform bias subtraction, flat-field correction, wavelength calibration, and spectral extraction on all other spectroscopic obser-

<sup>1</sup> <https://github.com/CIERA-Transients/POTPyRI>

vations. We apply a flux calibration to each spectrum using spectrophotometric standard spectra and co-add the flux-calibrated 1D spectra. We use the `PyPeIt`-measured spectral variance to determine spectral noise.

We correct all spectra for Galactic extinction using the Cardelli et al. (1989) extinction law and the  $V$ -band extinction in the direction of each host (Schlafly & Finkbeiner 2011). We identify high signal-to-noise ( $S/N > 5$ ) spectral features in each host spectrum and list the lines identified in Table A2. We confirm the previously published redshifts for all LFBOTs using the host galaxy lines, except for AT2020xnd, where we do not detect any spectral lines. We note that the redshift for AT2020xnd was determined from the detection of  $H\alpha$  (assumed to be from the host) in the transient spectrum (Perley et al. 2021).

### 3. STELLAR POPULATION MODELING

To determine the stellar population properties of our LFBOT host galaxy population, we fit their photometric and spectroscopic (if available) observations with stellar population modeling code, `Prospector` (Leja et al. 2019; Johnson et al. 2021). Within `Prospector`, we employ the nested sampling fitting routine `dynesty` to sample various combinations of stellar population properties of interest and produce their posterior distributions. `Prospector` creates model photometry and spectroscopy through `FSPS` (Flexible Stellar Population Synthesis) and `python-FSPS` (Conroy et al. 2009; Conroy & Gunn 2010), which internally uses the MILES spectral libraries (Falc3n-Barroso et al. 2011) and MIST models (Paxton et al. 2018).

For all `Prospector` fits, we use the Kriek & Conroy (2013) dust attenuation model, in which we sample an offset from the Calzetti et al. (2000) attenuation curve and the ratio of light attenuated from young ( $\tau_{V,1}$ ; in units of optical depth) to old ( $\tau_{V,2}$ ) stellar light, a Chabrier (2003) initial mass function (IMF), and the Draine & Li (2007) IR dust emission model, where we sample the polycyclic aromatic hydrocarbon mass fraction ( $q_{\text{pah}}$ ). We furthermore include a mid-IR Active Galactic Nuclei (AGN) model, with sampled parameters  $\tau_{\text{AGN}}$  (the mid-IR optical depth) and  $f_{\text{AGN}}$  (the total AGN luminosity, expressed as a fraction of the total bolometric luminosity from the host), although we note that only one host (AT2018cow) has well-sampled mid-IR data. To probe realistic combinations of total mass formed in the host ( $M_F$ ) and stellar metallicity ( $Z_*$ ), we impose the Gallazzi et al. (2005) mass-metallicity relation on their priors. Finally, we model the host star for-

mation history (SFH) with a seven-bin non-parametric continuity SFH model, with the first two bins linearly spaced from 0-30 Myr and 30-100 Myr and the last five bins log-spaced until the age of the Universe at each host’s redshift. We assume a constant star formation rate (SFR) in each bin and sample the ratio of the SFR between two adjacent bins.

For the nine LFBOT hosts with spectral line detections in their spectra, we model their spectral continua with a 12<sup>th</sup>-order Chebyshev polynomial and apply a spectral smoothing model to to normalize each host spectral continuum to its photometry. Given that the majority of our spectra are high  $S/N$ , we employ a noise inflation model that inflates the noise in all spectroscopic pixels to ensure that the spectra are not over-weighted in comparison to the photometry in the fit. We furthermore include a pixel outlier model, which marginalizes over poorly modeled noise in the spectra, like residual sky lines or missing absorption lines (see Appendix D in Johnson et al. 2021). We fit the spectral emission lines with a nebular marginalization template and sample a gas-phase metallicity ( $Z_{\text{gas}}$ ) and a dimensionless gas ionization parameter that measures the ratio of hydrogen ionizing photons density to hydrogen density ( $U_{\text{gas}}$ ). We note that we also include this nebular emission model hosts fits of AT2020xnd (in which we do not include the observed spectrum, as there are no identifiable features that would be useful in constraining the host stellar population properties) and AT2023vth, but we caution that this will likely result in poorly-constrained gas-phase metallicities, given that there are no spectral lines to fit. In all fits, we impose a 5% error floor on the photometry to avoid overfitting any single photometric measurement.

We finally convert several sampled parameters into more commonly-used physical galaxy properties. We calculate a mass-weighted age ( $t_m$ ) and present-day (0 – 100 Myr) SFR using the SFR ratios and  $M_F$ . We additionally determine  $M_*$  from  $M_F$ , the SFH, and  $Z_*$ . We lastly convert  $\tau_{V,1}$  and  $\tau_{V,2}$  to a total  $V$ -band dust extinction magnitude ( $A_V$ ) by multiplying their sum by 1.086. We present the LFBOT host galaxy stellar population properties in Table 1 and present the model fit to the observational data in Figure B1. We discuss these results in the following section.

### 4. STELLAR POPULATION PROPERTIES

In this section, we detail our main results from `Prospector` stellar population modeling of 11 LFBOT host galaxies. We focus this analysis on the stellar mass, star formation activity, and metallicities of the hosts and compare them to those of other transient host pop-

**Table 1.** Prospector Stellar Population Modeling Results

LFBOT	$z$	$\log(M_*/M_\odot)$	SFR [ $M_\odot \text{ yr}^{-1}$ ]	$\log(\text{sSFR})$ [ $\text{yr}^{-1}$ ]	Age [Gyr]	$\log(Z_*/Z_\odot)$	$\log(Z_{\text{gas}}/Z_\odot)$	$A_V$ [mag]	$\log(U_{\text{gas}})$
AT2018cow	0.0141	$9.41^{+0.02}_{-0.01}$	$0.27^{+0.12}_{-0.15}$	$-9.98^{+0.16}_{-0.34}$	$4.92^{+2.67}_{-0.95}$	$-0.28^{+0.02}_{-0.03}$	$-0.17^{+0.15}_{-0.19}$	$0.17^{+0.02}_{-0.02}$	$-2.41^{+0.32}_{-0.38}$
CSS161010	0.033	$7.6^{+0.11}_{-0.12}$	$0.05^{+0.02}_{-0.03}$	$-8.9^{+0.22}_{-0.36}$	$4.22^{+1.69}_{-2.08}$	$-1.55^{+0.21}_{-0.26}$	$-0.6^{+0.09}_{-0.08}$	$1.65^{+0.33}_{-0.29}$	$-3.97^{+0.04}_{-0.02}$
ZTF18abvkw1	0.2715	$9.85^{+0.17}_{-0.16}$	$23.42^{+11.0}_{-15.72}$	$-8.5^{+0.25}_{-0.49}$	$4.28^{+0.86}_{-0.7}$	$0.07^{+0.07}_{-0.07}$	$-0.6^{+0.05}_{-0.05}$	$3.76^{+0.23}_{-0.2}$	$-2.75^{+0.32}_{-0.19}$
AT2020mrf	0.1353	$8.24^{+0.05}_{-0.06}$	$0.05^{+0.03}_{-0.03}$	$-9.54^{+0.2}_{-0.44}$	$5.69^{+0.64}_{-0.82}$	$-0.88^{+0.12}_{-0.19}$	$-0.56^{+0.23}_{-0.13}$	$0.55^{+0.32}_{-0.19}$	$-3.69^{+0.23}_{-0.19}$
AT2020xnd	0.2433	$7.74^{+0.34}_{-0.4}$	$0.06^{+0.05}_{-0.03}$	$-8.99^{+0.51}_{-0.49}$	$3.41^{+1.95}_{-2.1}$	$-0.91^{+0.73}_{-0.69}$	$-0.6^{+0.24}_{-0.21}$	$0.36^{+0.55}_{-0.25}$	$-1.77^{+0.54}_{-0.66}$
AT2022tsd	0.2555	$9.64^{+0.15}_{-0.15}$	$1.74^{+3.15}_{-1.01}$	$-9.4^{+0.45}_{-0.41}$	$2.91^{+1.98}_{-1.59}$	$-0.88^{+0.2}_{-0.31}$	$-0.28^{+0.16}_{-0.15}$	$0.47^{+0.49}_{-0.29}$	$-3.06^{+0.18}_{-0.16}$
AT2023fhn	0.2375	$10.24^{+0.1}_{-0.15}$	$11.26^{+8.82}_{-5.38}$	$-9.17^{+0.29}_{-0.32}$	$4.85^{+0.89}_{-1.33}$	$-0.64^{+0.21}_{-0.19}$	$-0.81^{+0.04}_{-0.02}$	$1.03^{+0.46}_{-0.34}$	$-1.94^{+0.37}_{-0.29}$
AT2023hkw	0.335	$11.28^{+0.03}_{-0.04}$	$18.77^{+6.31}_{-7.47}$	$-10.01^{+0.13}_{-0.22}$	$5.37^{+0.48}_{-0.43}$	$0.15^{+0.03}_{-0.04}$	$-0.53^{+0.13}_{-0.11}$	$3.43^{+0.68}_{-0.34}$	$-2.43^{+0.49}_{-0.93}$
AT2023vth	0.0747	$9.94^{+0.08}_{-0.09}$	$16.56^{+13.27}_{-12.83}$	$-8.7^{+0.25}_{-0.66}$	$4.29^{+1.47}_{-1.01}$	$-0.93^{+0.07}_{-0.07}$	$-1.41^{+0.73}_{-0.41}$	$7.47^{+0.41}_{-0.32}$	$-2.73^{+0.83}_{-0.9}$
AT2024qfm	0.227	$10.37^{+0.05}_{-0.04}$	$3.82^{+1.69}_{-1.26}$	$-9.79^{+0.17}_{-0.18}$	$5.98^{+0.53}_{-0.55}$	$0.17^{+0.01}_{-0.02}$	$-0.66^{+0.09}_{-0.05}$	$0.8^{+0.36}_{-0.22}$	$-2.08^{+0.28}_{-0.26}$
AT2024wpp	0.0866	$8.86^{+0.06}_{-0.05}$	$0.03^{+0.09}_{-0.01}$	$-10.4^{+0.62}_{-0.28}$	$4.07^{+1.57}_{-1.71}$	$-1.78^{+0.05}_{-0.07}$	$-0.43^{+0.13}_{-0.19}$	$0.15^{+0.11}_{-0.12}$	$-3.44^{+0.13}_{-0.14}$
All	$0.23^{+0.03}_{-0.17}$	$9.61^{+0.74}_{-1.61}$	$0.95^{+18.37}_{-0.91}$	$-9.49^{+0.81}_{-0.66}$	$4.73^{+1.36}_{-1.3}$	$-0.74^{+0.88}_{-0.81}$	$-0.59^{+0.3}_{-0.21}$	$0.9^{+2.86}_{-0.72}$	$-2.75^{+0.81}_{-0.97}$

NOTE—The redshifts and **Prospector**-determined stellar masses ( $M_*$ ), SFRs, specific SFRs (sSFR), mass-weighted stellar population age, stellar metallicities ( $Z_*$ ), gas-phase metallicities ( $Z_{\text{gas}}$ ), dust extinction ( $A_V$ ), and gas ionization parameter ( $U_{\text{gas}}$ ) for our LFBOT host population.

ulations. In Section 4.1, we discuss the LFBOT host  $M_*$  distributions, SFHs, and present-day star formation properties. We furthermore explore LFBOT hosts on a 2D SFR- $M_*$  plane. In Section 4.2, we cover the stellar and gas-phase LFBOT hosts metallicities, as well as their gas-phase oxygen abundances and where they lie on the Baldwin, Phillips and Telervich (BPT) diagram.

#### 4.1. Mass and Star Formation

We begin our analysis of LFBOT host stellar population properties by examining their host stellar masses and star formation properties. We show cumulative distributions (CDFs) of LFBOT host  $M_*$  and present-day specific SFR (sSFR = SFR/ $M_*$ ) in Figure 1. To build the distributions, we sample (with replacement) 100,000 values from each LFBOT host’s **Prospector**-derived stellar population property posterior distributions and create 100,000 realizations on the CDF. We find that LFBOT hosts have  $\log(M_*/M_\odot) = 9.61^{+0.74}_{-1.61}$  (median and 68% interval), present-day SFR =  $0.95^{+18.37}_{-0.91} M_\odot \text{ yr}^{-1}$ , and sSFR =  $-9.49^{+0.81}_{-0.66} \text{ yr}^{-1}$ . We further characterize the transients as star-forming, quiescent, or transitioning between either state using Equation (2) in Tacchella et al. (2022), which depends on the galaxy’s sSFR and age of the Universe at the galaxy’s redshift. We determine that all LFBOT host galaxies are actively star-forming galaxies.

Despite the apparent uniformity in present-day star-formation classification, it appears that LFBOT hosts have a diverse array of SFH shapes, which we highlight in Figure 2. We see that four hosts are still actively rising in SFR until present-day (hosts of CSS161010, ZTF18abvkw1, AT2020xnd, and AT2023hkw), and the

other hosts have had past burst(s) of star formation, and have since declined or plateaued in SFR (hosts of AT2018cow, AT2020mrf, AT2022tsd, AT2023fhn, AT2023vth, AT2024qfm, And AT2024wpp). We note that the majority of hosts have had a star-formation burst or have reached their highest SFR in the past  $\approx 100$  Myr (with the exception of AT2024wpp, which appears to have had a single star formation burst  $\approx 1$  Gyr ago). If LFBOTs are of stellar origin (see Section 6 for further discussion), and assuming their progenitor has the highest probability of forming in the most recent burst of star formation, this likely implies that their progenitor formation timescale (delay time) is relatively short.

To contextualize the  $M_*$  and sSFRs of the LFBOT host population, we compare them to other well-studied transient populations that LFBOTs have been frequently compared to in the literature: SLSNe-I, Type II SNe (SNe II), Type Ibc SNe (SNe Ibc), Type Ibn SNe (SNe Ibn), and LGRBs. We obtain host galaxy sSFRs and  $M_*$  for SNe II, Ibc, and Ibn in Nugent et al. (2026), LGRBs in Svensson et al. (2010); Perley & Perley (2013); Wang & Dai (2014); Niino et al. (2017), and SLSNe-I in Schulze et al. (2021). We note that Nugent et al. (2026) employed the same **Prospector** model as used in this work to derive host stellar population properties (minus the parameters used to fit the spectrum as they only employed host photometry in their study), thus their results are complementary to the ones derived here. Schulze et al. (2021) also adopted a **Prospector** model to determine SLSN-I host  $M_*$  and sSFR, however, they modeled SFH with a parametric delayed- $\tau$  model. As shown in Leja et al. (2019), non-parametric

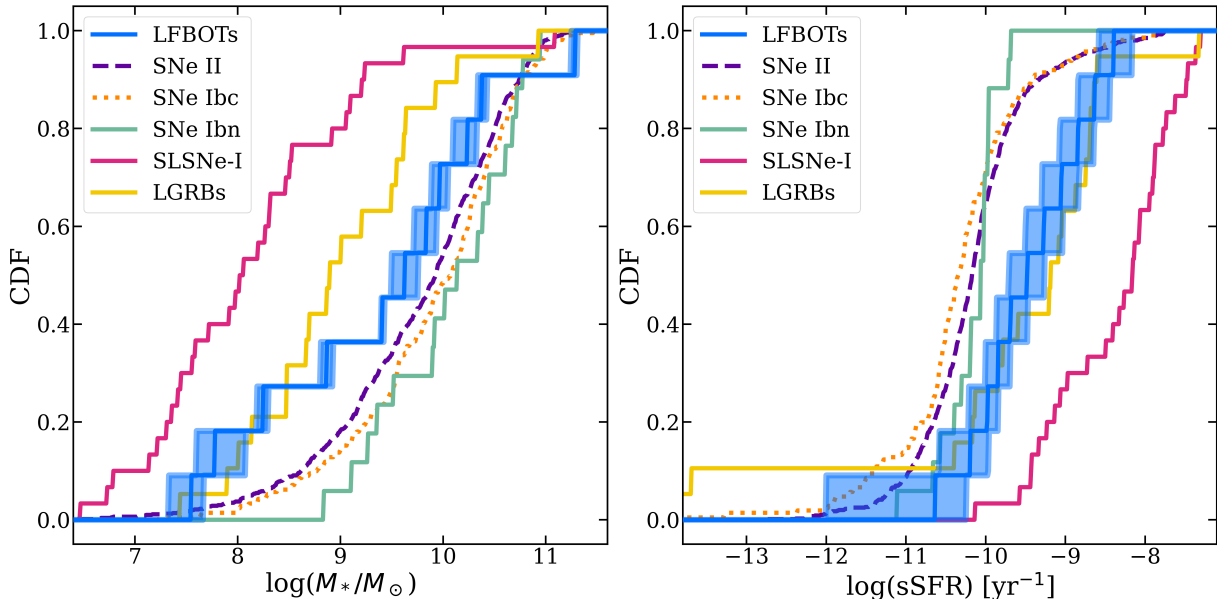


**Figure 1.** *Left:* The stellar mass CDFs for the hosts of LFBOTs (blue; median and 68% interval), SNe II (purple dashed line), SNe Ibc (orange dotted line), SNe Ibn (green), SLSNe-I (pink), and LGRBs (yellow). LFBOT hosts are more massive than those of SLSNe-I and have statistically similar stellar mass distributions to SNe Ibc, Ibn, II and LGRB hosts. *Right:* The sSFR CDFs for the same transient populations. LFBOT hosts are less star-forming than SLSNe-I hosts, and more star-forming than CCSNe (SNe II, Ibc, and Ibn) hosts. Their hosts’ sSFR distribution is not statistically distinct from that of LGRB hosts.

SFH models (used here) tend to result in stellar masses that are 25–100% larger than those returned by parametric SFH models and may lead to subtle differences in present-day SFRs. In turn, there may be slight systematic differences between the LFBOT and SLSNe-I  $M_*$  and sSFR distributions caused by these varying methods. This also may be the case for the LGRB host sample, as Svensson et al. (2010), Perley & Perley (2013), Wang & Dai (2014), and Niino et al. (2017) use a variety of stellar population modeling techniques to derive LGRB host properties. Finally, we note that redshift may also bias comparisons between LFBOT host properties and the other samples. For example, at higher redshift, we expect that galaxy populations will have lower  $M_*$  and higher sSFR. To mitigate this redshift effect, we limit all host samples to  $z < 0.5$ <sup>2</sup>, where we expect that redshift will have a subtler effect on the overall  $M_*$  and sSFR distributions.

In Figure 1, we compare CDFs of these transient host stellar population in  $M_*$  and sSFR. Compared to the selected transient populations, it seems that LFBOT hosts are more massive and less star-forming than SLSNe-I hosts, have similar stellar masses and sSFRs to LGRB hosts, and are less massive and more star-forming than the CCSNe host populations. To quantitatively compare

LFBOT  $M_*$  and sSFR distributions to those of these selected transient populations, we perform Anderson-Darling (AD) rejection tests, with the null hypothesis that LFBOTs and the transient-of-interest derive from the same underlying stellar mass or sSFR distribution. For each LFBOT-transient pair, we perform 10,000 AD tests, with each test between one randomly-selected realization on the LFBOT  $M_*$  or sSFR distribution and the respective transient  $M_*$  or sSFR distribution. We then determine the percentage of tests that fall below probability  $P_{AD} < 0.05$ , the point at which we can reject the null hypothesis. If  $> 50\%$  of tests result in  $P_{AD} < 0.05$ , we reject the null hypothesis.

As suspected, we find that we cannot reject the null-hypothesis that LFBOTs trace the same  $M_*$  or sSFR distributions as LGRBs, given that 0% of  $P_{AD} < 0.05$  when testing both properties. We furthermore verify that LFBOT  $M_*$  and sSFRs are statistically distinct from those of SLSNe (100% of  $P_{AD} < 0.05$  for both  $M_*$  and sSFR). Given the stark difference in the LFBOT and SLSNe-I host  $M_*$  and sSFR distributions, we do believe that this distinction is real and not heavily biased by subtle differences in the stellar population modeling technique. While we also validate that LFBOT hosts trace higher sSFRs than SNe II, Ibc, and Ibn ( $> 96\%$  of  $P_{AD} < 0.05$  for all three comparisons), their stellar mass distributions are not statistically different ( $< 6\%$  of  $P_{AD} < 0.05$  for all three comparisons). Thus, it ap-

<sup>2</sup> This redshift limit only affects the SLSNe-I and LGRB samples, which contain many more events at  $z > 0.5$ . The CCSNe populations exclusively lie at  $z < 0.2$ .

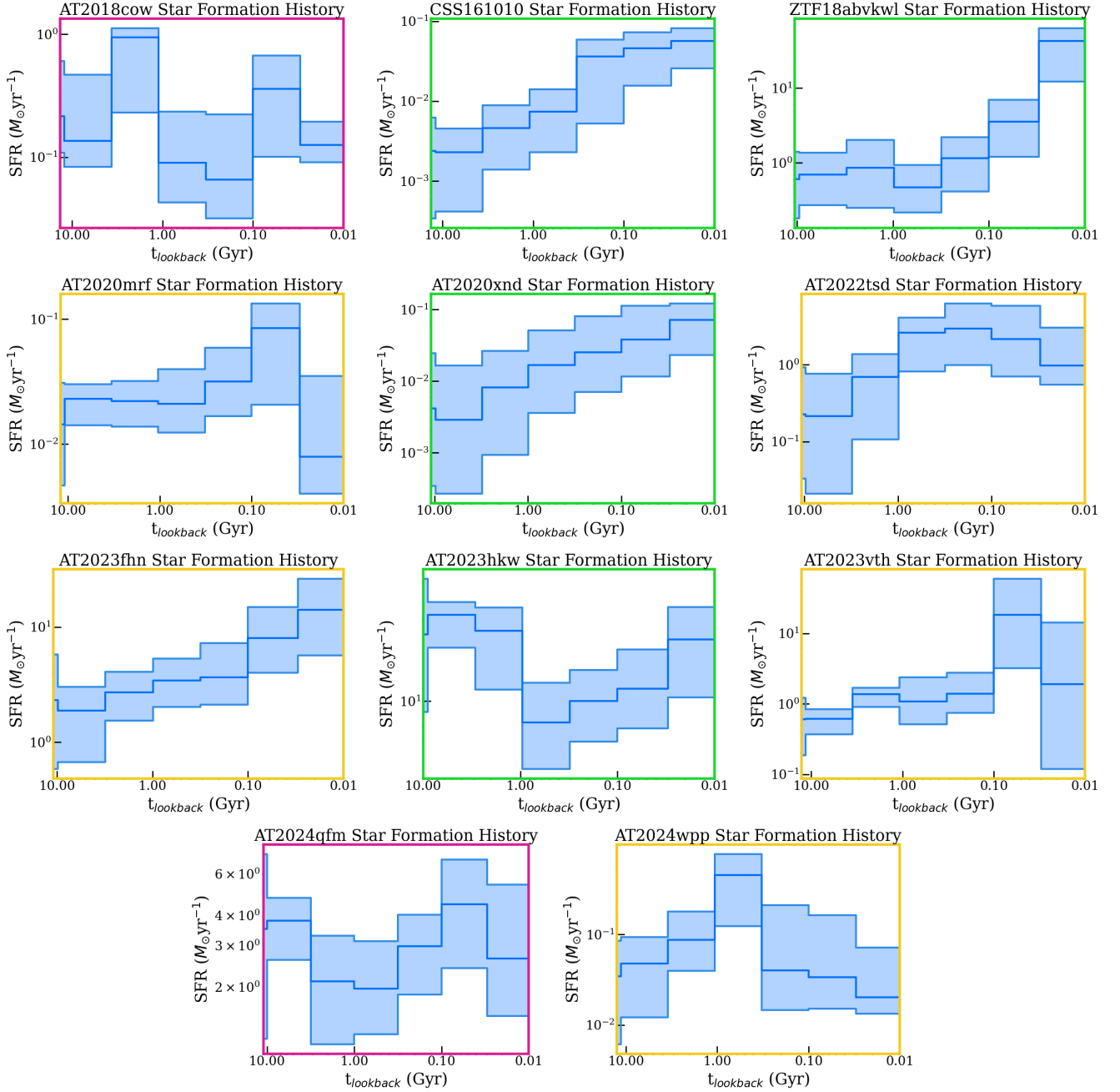


**Figure 2.** The Prospector-derived SFHs of the 11 LFBOT hosts in our sample. We see a diversity of SFH shapes: four events have clearly rising SFHs (green border) and the rest appear to have had one (yellow border) or several (pink border) star formation bursts in their past have since declined or plateaued in SFR. All hosts are currently star-forming.

pears that LFBOT hosts may be more star-forming than CCSN hosts but are not distinct in stellar mass.

As another test of how different LFBOT hosts are from the selected transient hosts, we showcase them along the star-forming main-sequence (SFMS) in Figure 3: a well-studied galaxy relation followed by star-forming galaxies as they gain in stellar mass (Speagle et al. 2014; Whitaker et al. 2014; Leja et al. 2022). How transient hosts track the SFMS informs how dependent

their progenitors are on star-formation or stellar mass for formation (with older progenitors more dependent on stellar mass, given their longer formation timescales). Visually, it appears that LFBOT hosts trace the SFMS and are “normal” star-forming galaxies, similar to the CCSN populations. On the contrary, SLSN and LGRB hosts appear to lie above the SFMS (Schulze et al. 2018, 2021).

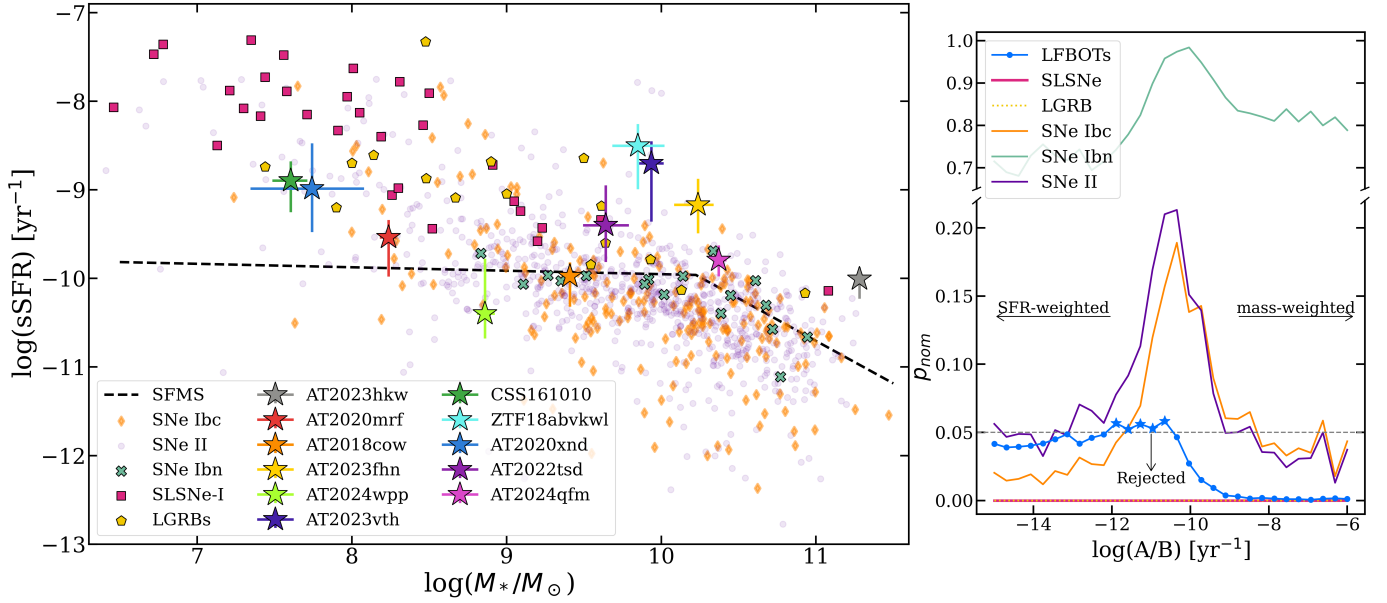


**Figure 3.** *Left:* The hosts of LFBOTs (stars; lines indicate median and 68% interval), SNe II (purple circles), SNe Ibc (orange diamonds), SNe Ibcn (green crosses), SLSNe-I (pink squares), and LGRBs (yellow pentagons) along the SFMS derived in [Leja et al. \(2022\)](#). LFBOTs hosts lie along the SFMS, similar to the CCSNe host populations, and are clearly distinct from LGRB and SLSN-I hosts. *Right:* The results of the [Horowitz & Margalit \(2026\)](#) test, which determines if a host galaxy population is drawn from a weighted SFR- $M_*$  distribution of a mock field galaxy population. We determine weights from  $\log(A/B)$ , where lower values indicate more SFR-weighted distributions, and higher values indicate more  $M_*$ -weighted distributions. If  $p_{\text{nom}} < 0.05$ , we can reject the null hypothesis that the host galaxy sample is drawn from the weighted distribution. We find that LFBOT hosts prefer more SFR-weighted distributions, especially in comparison the SNe II and Ibc hosts. The stars mark the solutions where the LFBOT 1D SFR and  $M_*$  distributions were not statistically distinct from those of the weighted distribution. We cannot reject any weighted distributions for SNe Ibcn hosts and we do not find any solution that fits the SFR- $M_*$  distributions of LGRB and SLSN-I hosts well.

As a more quantitative assessment of how LFBOT hosts track the SFMS, we next determine how LFBOTs track both SFR and  $M_*$  in the 2D SFR- $M_*$  plane, given the multivariate statistical test presented in [Horowitz & Margalit \(2026\)](#). In other words, we test the relative rate of LFBOTs tracking SFR or  $M_*$  to determine how dependent their progenitor may be on either of these properties for formation. The [Horowitz & Margalit \(2026\)](#) test was applied in [Nugent et al. \(2026\)](#) for several SN host populations (including SNe II and Ibc) and essentially determines if an observed host galaxy sample SFR- $M_*$  distribution are drawn from that of a weighted mock galaxy population. To begin, we draw 32,000 mock galaxy SFRs and  $M_*$  from weighted probability density distributions,  $W \times \rho(M_*, \text{SFR}|z)$ , at each LFBOT host redshift. Weights are given by:

$$W_i = A \left( \frac{M_{*,i}}{M_\odot} \right) + B \left( \frac{\text{SFR}_i}{M_\odot \text{yr}^{-1}} \right), \quad (1)$$

where if  $A \rightarrow 0$ , the solution reduces to a SFR-weighted distribution, and if  $B \rightarrow 0$ , the solution reduces to a  $M_*$ -weighted distribution. The “unweighted” probability density is based on the observed COSMOS2015 ([Laigle et al. 2016](#)) and 3D-HST ([Skelton et al. 2014](#)) galaxy

SFR- $M_*$  distribution determined in [Leja et al. \(2022\)](#). [Horowitz & Margalit \(2026\)](#) formulate a rejection test to determine whether a weighted distribution can be ruled out to describe the SFR- $M_*$  distribution of a transient host population. Similar to the AD test, they determine a nominal  $p$ -value ( $p_{\text{nom}}$ ), where  $p_{\text{nom}} < 0.05$  suggests the null hypothesis that the transient hosts derive from a specified weighted distribution can be rejected. For more details on this method, we refer the readers to [Horowitz & Margalit \(2026\)](#).

We perform the [Horowitz & Margalit \(2026\)](#) rejection test on LFBOT hosts for 30 weighted distributions from  $-15 \leq \log(A/B) \leq -6$ , where  $A + B = 1$ . We determine a single  $p_{\text{nom}}$  for each weighted distribution, using only the median SFRs and  $M_*$  of our LFBOT host population. In addition, we do the same tests for LGRB,

SLSN-I, and SN Ibn host populations as these do not exist in the literature<sup>3</sup>.

We show the results of the rejection test in Figure 3. We find that we can reject the most mass-weighted SFR- $M_*$  distributions for LFBOTs, with their hosts seemingly preferring more SFR-weighted solutions but not the most SFR-weighted distributions. As another test of whether the 2D weighted distribution fits the LFBOT host galaxy SFR- $M_*$  distribution well, we perform Kolmogorov-Smirnov (KS) tests between the 1D LFBOT and weighted SFR and  $M_*$  distributions<sup>4</sup>. To encapsulate uncertainty on the LFBOT SFR and  $M_*$  distributions in the KS tests, we randomly sample 10,000 realizations on their SFR and  $M_*$  CDFs. We reject the null hypothesis in the same manner as the AD tests described previously. We find that we cannot reject the null hypothesis that LFBOTs trace the same 1D  $M_*$  and SFR distributions as the weighted mock galaxy sample with  $-11.9 \lesssim \log(A/B) \lesssim -10.6$ , implying LFBOTs do indeed trace more SFR-weighted distributions in both the 1D and 2D tests.

The LFBOT host preference for more SFR-weighted SFR- $M_*$  distributions is distinct from the other transient host populations. In Figure 3, it is apparent that SNe II and Ibc hosts prefer more  $M_*$ -weighted solutions than LFBOTs (however, these solutions are still relatively SFR-weighted), likely owing to their larger populations of more massive hosts with lower SFRs. Interestingly, we cannot find any SFR or  $M_*$ -weighted distribution that LGRBs or SLSNe-I prefer. This is almost certainly due their hosts lying well above the SFMS and being highly star-forming galaxies. Moreover, SLSN-I and LGRB progenitors are likely more dependent on metallicity than either SFR or  $M_*$  (see Section 4.2). Importantly, this highlights that LFBOTs trace a separate low-mass, star-forming galaxy population than either of these transients, implying that their progenitor is dependent on different environmental factors for formation. We further note that we cannot rule out any solutions for SNe Ibn, as their hosts span a range of  $M_*$  and SFR, with no obvious high-density region in the SFR- $M_*$  plane. This mitigates any reasonable compari-

<sup>3</sup> For the SN Ibn host population, we employ the same methods as described in Nugent et al. (2026), where they used a weighted distribution with an optical bias to exclude any mock galaxies with optical magnitude  $>23.5$  mag (the same bias as their SN host sample). We do not use this bias for LFBOTs, LGRBs, and SLSNe as their host populations include galaxies fainter than this limit.

<sup>4</sup> We choose KS over AD tests in this scenario as the speed of the KS test allows us to more quickly compare the LFBOT hosts to the large simulated galaxy population.

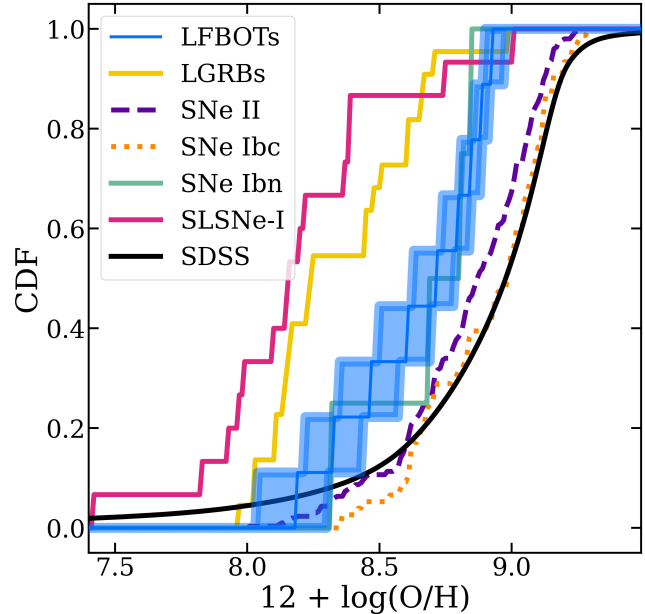


**Figure 4.** CDFs of the gas-phase oxygen abundances ( $12+\log(\text{O}/\text{H})$ ) for LFBOT hosts (blue), LGRBs (yellow), SNe II (purple dashed line), SNe Ibc (orange dotted line), SNe Ibn (green), SLSNe-I (pink), and a field galaxy population from SDSS (black). LFBOT hosts are clearly more metal-rich than SLSNe-I and LGRB hosts and more metal-poor than SNe Ibc and II hosts. In addition, LFBOTs trace lower metallicities than the field galaxy population.

son we can achieve between LFBOT and SNe Ibn hosts with this 2D test.

Overall, we conclude that LFBOTs prefer more star-forming hosts than most CCSN sub-types, but are less star-forming and not as low mass as SLSN-I hosts. Moreover, LFBOTs seemingly trace more “normal” low mass, star-forming galaxies along the SFMS than either LGRBs or SLSNe-I, hinting that their progenitor has a separate formation pathway and environmental dependencies.

#### 4.2. Metallicity

We next explore the metallicities of our LFBOT host population. We generally find that LFBOT host stellar and gas-phase metallicities are subsolar, leaning towards low-metallicity values, with median and 68% intervals of  $\log(Z_*/Z_\odot) = -0.74^{+0.88}_{-0.81}$  and  $\log(Z_{\text{gas}}/Z_\odot) = -0.59^{+0.3}_{-0.21}$ . As many studies on general field galaxy populations and other transient host populations use gas-phase oxygen abundance metallicities ( $12 + \log(\text{O}/\text{H})$ ), we additionally determine this metallicity measurement for our LFBOT host population. We compute  $12 + \log(\text{O}/\text{H})$  for LFBOT hosts with

**Table 2.** LFBOT Host Metallicities

LFBOT	$12 + \log(\text{O}/\text{H})$	$12 + \log(\text{O}/\text{H})$	$\log([\text{OIII}]/\text{H}\beta)$	$\log([\text{NII}]/\text{H}\alpha)$	$\log([\text{SII}]/\text{H}\alpha)$	$\log([\text{OI}]/\text{H}\alpha)$
	$R_{23}$	$[\text{NII}]/\text{H}\alpha$				
AT2018cow	$8.7^{+0.08}_{-0.09}$	...	$0.38^{+0.15}_{-0.15}$	$-0.87^{+0.14}_{-0.14}$	$-0.84^{+0.16}_{-0.16}$	$-1.84^{+0.21}_{-0.21}$
CSS161010	...	$8.28^{+0.09}_{-0.1}$	$0.48^{+0.13}_{-0.12}$	$-0.82^{+0.14}_{-0.14}$	$-0.17^{+0.07}_{-0.07}$	$-1.07^{+0.08}_{-0.08}$
ZTF18abvkw1	$8.89^{+0.04}_{-0.04}$	...	$0.59^{+0.23}_{-0.23}$	$-1.18^{+0.12}_{-0.12}$	$-0.75^{+0.1}_{-0.1}$	$-1.78^{+0.12}_{-0.12}$
AT2020mrf	$8.33^{+0.13}_{-0.15}$	$8.36^{+0.22}_{-0.24}$	$-0.54^{+0.37}_{-0.37}$	$-0.79^{+0.34}_{-0.34}$	$-0.28^{+0.21}_{-0.21}$	$-1.2^{+0.27}_{-0.27}$
AT2022tsd	$8.52^{+0.08}_{-0.1}$	$8.61^{+0.17}_{-0.18}$	$0.19^{+0.18}_{-0.18}$	$-0.63^{+0.2}_{-0.2}$	$-0.47^{+0.12}_{-0.12}$	$-1.49^{+0.15}_{-0.15}$
AT2023fhn	$8.84^{+0.04}_{-0.06}$	...	$0.67^{+0.14}_{-0.14}$	$-1.29^{+0.15}_{-0.15}$	$-1.06^{+0.12}_{-0.12}$	$-2.03^{+0.13}_{-0.13}$
AT2023hkw	$8.88^{+0.08}_{-0.18}$	...	$0.7^{+0.21}_{-0.21}$	$-1.27^{+0.16}_{-0.16}$	$-0.86^{+0.15}_{-0.15}$	$-1.87^{+0.18}_{-0.18}$
AT2024qfm	$8.85^{+0.04}_{-0.06}$	...	$0.74^{+0.13}_{-0.13}$	$-1.59^{+0.16}_{-0.16}$	$-1.09^{+0.1}_{-0.1}$	$-2.04^{+0.12}_{-0.12}$
AT2024wpp	$8.31^{+0.14}_{-0.17}$	$8.42^{+0.18}_{-0.19}$	$-0.19^{+0.2}_{-0.2}$	$-0.67^{+0.22}_{-0.22}$	$-0.32^{+0.14}_{-0.14}$	$-1.3^{+0.16}_{-0.16}$

NOTE—Different emission-line measured metallicity estimates for the LFBOT hosts with observed spectra used in their **Prospector** fits. For LFBOT hosts that have a median  $R_{23}$ -determined  $12 + \log(\text{O}/\text{H}) < 8.53$ , we use their  $[\text{NII}]/\text{H}\alpha$ -determined metallicity. We do not calculate an  $R_{23}$ -based metallicity for the host of CSS161010, as the  $[\text{OIII}]$  and  $\text{H}\beta$  fluxes were not well-constrained in the **Prospector** fit.

emission line flux measurements determined through our **Prospector** fitting<sup>5</sup> using the  $R_{23}$  calibration method, wherein:

$$R_{23} = \log_{10} \left( \frac{\text{OIII}\lambda\lambda 3727, 3729 + \text{OIII}\lambda\lambda 4959, 5007}{\text{H}\beta} \right). \quad (2)$$

We then follow the methodology in Kewley et al. (2019) (see Table 3) to determine  $12 + \log(\text{O}/\text{H})$ , which is dependent on  $R_{23}$  and  $\log(U_{\text{gas}})$ . To correctly capture the uncertainty on each  $12 + \log(\text{O}/\text{H})$  measurement, we sample 1000 emission line fluxes for each line in Equation 2 from an asymmetric Gaussian distribution, using the 68% interval on the flux provided by **Prospector**, and thus collect 1000  $R_{23}$  and  $12 + \log(\text{O}/\text{H})$  values. We note that we only use the median  $\log(U_{\text{gas}})$ , as provided in Table 1. We present the median and 68% interval on the  $R_{23}$ -determined  $12 + \log(\text{O}/\text{H})$  measurement for each LFBOT host in Table 2. As highlighted in Kewley et al. (2019), the  $R_{23}$  method is only valid at higher metallicities:  $8.53 < 12 + \log(\text{O}/\text{H}) < 9.23$ . Thus, for the hosts with  $R_{23}$ -determined metallicities below this limit, we additionally calculate  $12 + \log(\text{O}/\text{H})$  from the  $[\text{NII}\lambda 6584]/\text{H}\alpha$  ratio, given the equation in Kewley et al. (2019), Table 2, which is valid over  $7.63 < 12 + \log(\text{O}/\text{H}) < 8.53$ . We model uncertainties for this metallicity calibration method in the same manner as described for the  $R_{23}$  method and also show these results in Table 2. We use the  $[\text{NII}]/\text{H}\alpha$ -derived metallic-

ity for all low metallicity LFBOT hosts, and the  $R_{23}$ -determined metallicity for all other hosts.

In Figure 4 we highlight the LFBOT  $12 + \log(\text{O}/\text{H})$  CDF (the median and 68% interval are built from 10,000 realizations on the CDF). We determine that LFBOTs have a population median and 68% interval  $12 + \log(\text{O}/\text{H}) = 8.71^{+0.17}_{-0.40}$ . To contextualize these results, we compare them to a general field galaxy population from the Sloan Digital Sky Survey (SDSS) Data Release 7 (Tremonti et al. 2004; Abazajian et al. 2009), a population of SN II, Ibc, and Ibn hosts from Qin & Zabludoff (2024), LGRB hosts from Wang & Dai (2014), and SLSN-I hosts from Perley et al. (2016). We show CDFs of each of these galaxy samples in Figure 4, as well. Visually, it appears that LFBOT hosts are more metal-rich than SLSN-I and LGRB hosts, but more metal-poor than SN II and Ibc hosts and the general field galaxy populations. LFBOTs and SNe Ibn appear to have very similar  $12 + \log(\text{O}/\text{H})$  distributions. As we have done with stellar mass and sSFR, we determine if there are statistically significant differences in these distributions using AD tests. We perform 10,000 AD tests between a single realization on the LFBOT  $12 + \log(\text{O}/\text{H})$  CDF and that of the galaxy population of interest. Aligned with our expectations, we find that we can reject the null hypothesis that LFBOTs trace the same  $12 + \log(\text{O}/\text{H})$  distribution as the hosts of SLSNe-I (98% of  $P_{AD} < 0.05$ ), LGRBs (90% of  $P_{AD} < 0.05$ ), SNe Ibc (100% of  $P_{AD} < 0.05$ ), and SNe II (62% of  $P_{AD} < 0.05$ ). We furthermore find statistical support that LFBOT hosts are more metal-poor than the general field galaxy population, as 99% of  $P_{AD} < 0.05$ . We do not find any statistical distinction between the dis-

<sup>5</sup> We exclude the hosts of AT2020xnd and AT2023vth from this analysis, as we did not use spectra in their **Prospector** fits.

tributions of LFBOTs and SNe Ibn (as expected; 0% of  $P_{AD} < 0.05$ ). We, do however, find that we cannot reject the null hypothesis that SNe Ibn trace the same metallicity distributions as the other CCSN hosts; thus, it is possible that small number statistics is playing a role in the outcome of our tests.

As a further test of the metallicity dependence of LFBOTs, we place their hosts on the BPT diagram, typically used to separate star-forming galaxies and AGN (Baldwin et al. 1981; Veilleux & Osterbrock 1987; Kewley et al. 2001, 2006; Kauffmann et al. 2003). In Figure 5, we highlight three variations of the BPT diagram:  $\log(\text{OIII}/\text{H}\beta)$  versus  $\log(\text{NII}/\text{H}\alpha)$ ,  $\log(\text{SII}/\text{H}\alpha)$ , and  $\log(\text{OI}/\text{H}\alpha)$ , along with the Kewley et al. (2006) and Cid Fernandes et al. (2010) star-forming galaxy-AGN demarcation lines. For all LFBOT hosts with spectra, we present the median and 68% interval on these emission line ratios in Table 2<sup>6</sup>. For the host of CSS161010, we do not use the *Prospector*-determined emission line fluxes for  $[\text{OIII}\lambda 5007]$  and  $\text{H}\beta$ , as the model fit determined a higher  $\text{H}\beta$  flux density than  $[\text{OIII}\lambda 5007]$ , when this is clearly not the case from examining the host spectrum (see Figure B1). Instead, we subtract its observed spectrum from the spectral continuum model output by *Prospector* and estimate emission line flux densities by fitting the lines with a Gaussian function and integrating under the curves. We use the spectral noise to determine error. We do not find similar issues when examining other lines in its spectrum or the *Prospector* model fits to other hosts; thus, this problem is unique to the CSS161010 host fit and likely caused by the fact that these lines are so weakly detected in the host spectrum.

As a point of comparison in the BPT diagrams, we additionally plot the SDSS field galaxy sample (Abazajian et al. 2009), SLSNe-I host sample from Perley et al. (2016), LGRB host sample from Niino et al. (2017), and CCSNe (II, Ibc, and In) host samples from Qin & Zabludoff (2024) in Figure 5. In all three BPT diagrams, LFBOT hosts appear to trace the line that separates star-forming galaxies and AGN, lying slightly above the bulk of the SDSS field galaxies. We note that this does not indicate the presence of AGN in their hosts, as the majority clearly still fall in the star-forming phase space. Even the host of CSS161010, which lies in the AGN region of the  $[\text{SII}]$  and  $[\text{OI}]$  BPT diagrams, is likely not being affected by an AGN, as Coppejans et al. (2020) re-

ported no AGN activity in the host. Instead, this probably hints that LFBOT hosts are more ionized (higher  $U_{\text{gas}}$ ) than the normal field galaxy population, which can shift the star-forming sequence of galaxies towards higher  $[\text{OIII}]/\text{H}\beta$  ratios (Brinchmann et al. 2008; Kewley et al. 2013, 2019). Indeed, we do find that the LFBOT host median gas ionization parameter  $\log(U_{\text{gas}}) \approx -2.75$  is higher than predicted for normal field galaxy populations, where  $-3.2 \lesssim \log(U_{\text{gas}}) \lesssim -2.9$  (Kewley & Dopita 2002; Nakajima & Ouchi 2014; Kaasinen et al. 2018). Higher ionization levels in galaxies are likely due to more compact, extreme star formation, a more top-heavy IMF, a larger WR star population, and/or lower metallicity (Kewley et al. 2001; Brinchmann et al. 2008). As we have shown, LFBOT hosts are more metal-poor and more SFR-weighted than normal field galaxy populations, suggesting this is the most likely cause of their divergence from the field galaxy population on the BPT diagrams. Interestingly, we also find that LFBOT hosts appear distinct from CCSN hosts, which, in general, appear to trace the same phase-space as the field galaxy population. On the other hand, LFBOT hosts trace similar regions in the BPT diagrams as SLSN-I hosts and LGRBs: transients that have a strong-metallicity dependence and occur in galaxies with more extreme sSFRs than the CCSN populations.

Overall, we infer that LFBOTs do appear to have a metallicity dependence, preferring environments that are on-average more metal-poor than those of typical CCSN hosts and the general field galaxy population. However, their hosts do not appear to as metal-poor as those of SLSNe-I and LGRBs, suggesting that they have different progenitors. We discuss further implications on LFBOT origins in Section 6.

#### 4.3. Comparisons to Previous LFBOT Literature

We next briefly compare our main stellar population modeling results to those previously derived in other literature. We first emphasize that our study takes advantage of all available host galaxy photometry and spectroscopy and sophisticated, uniform stellar population modeling techniques to place the best constraints on LFBOT environments. Thus, our results should be compared to in all future analyses of LFBOT environments. We find estimates of host galaxy stellar mass and SFR for 9 LFBOTs in our sample: AT2018scow (Perley et al. 2019), CSS161010 (Coppejans et al. 2020), ZTF18abvkw (Ho et al. 2020), AT2020mrf (Yao et al. 2022), AT2024wpp (Perley et al. 2026), AT2023fhn, AT2023hkw, AT2023vth, and AT2024qfm (Sevilla et al. 2026). We note that the stellar population modeling techniques employed across these papers is inconsistent

<sup>6</sup> Ho et al. (2020) and Yao et al. (2022) also determined host galaxy emission line fluxes and/or ratios for the hosts of ZTF18abvkw and AT2020mrf, respectively, using various line fitting techniques. Our *Prospector*-determined emission line ratios are consistent within error to their findings.

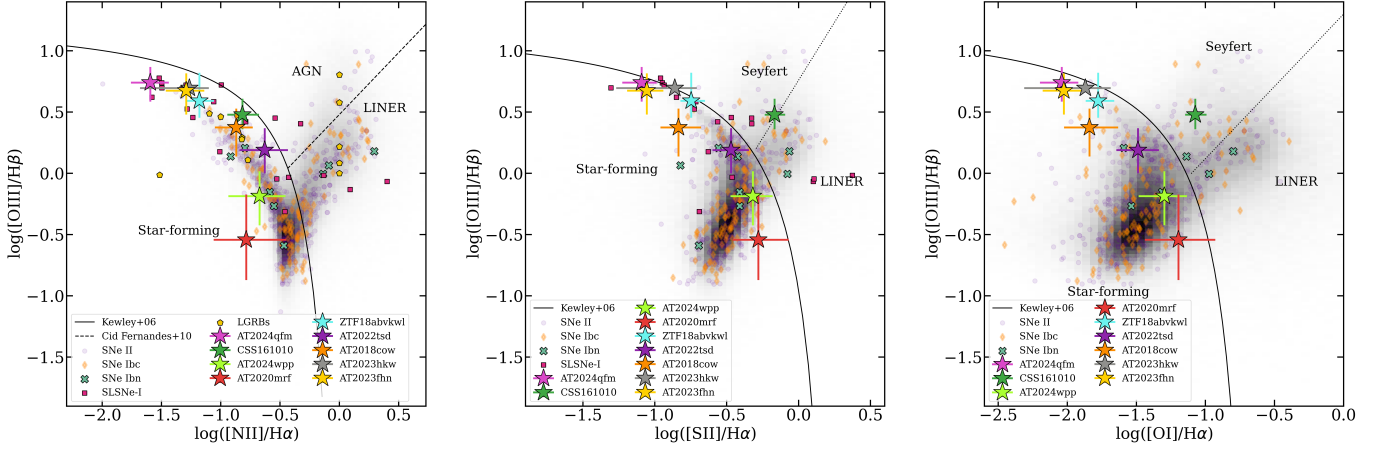


**Figure 5.** Three variations of the BPT diagram:  $[\text{OIII}]/\text{H}\beta$  versus  $[\text{NII}]/\text{H}\alpha$  (left),  $[\text{SII}]/\text{H}\alpha$  (center),  $[\text{OI}]/\text{H}\alpha$  (right), with the Kewley et al. (2006) and Cid Fernandes et al. (2010) star-forming galaxy-AGN demarcation line over-plotted. LFBOT hosts are indicated with stars, SLSNe-I are represented by pink squares, LGRB hosts by yellow pentagons, SNe II hosts with purple circles, SNe Ibc hosts with orange diamonds, and SNe Ibn hosts with green crosses. We also show a field galaxy population from SDSS (grey histogram). In all three BPT diagnostics, LFBOTs appear to lie at higher  $[\text{OIII}]/\text{H}\beta$  ratios than the field galaxy population and CCSN hosts, and occur in a more similar phase-space as SLSNe-I and LGRB hosts. This is likely caused by increased ionization in the LFBOT, SLSNe-I, and LGRB hosts due to higher amounts of star-formation, lower metallicities, and/or a larger massive star population.

and generally focus on fitting host photometry exclusively, which will give poorer constraints on SFR than achieved here. Moreover, the majority of these studies rely on parametric SFH models. As previously explained, this tends to lead to lower stellar mass estimates and differing SFR constraints than the non-parametric SFH model. Indeed, we determine higher stellar masses for 8 LFBOTs in this sample (all except AT2024wpp). On average, the increase is  $\approx 0.3$  dex. The most extreme differences are for ZTF18abvkw and AT2023vth, where we find stellar masses that are  $\approx 1$  dex higher than those published in Ho et al. (2020) and Sevilla et al. (2026), respectively. This is almost certainly due to our usage of a non-parametric SFH model and, in the case of ZTF18abvkw, jointly fitting both the host photometry and spectrum in the SED fit.

The majority of our SFR measurements are consistent with those that were previously published, and we find only minimally higher SFRs for CSS161010, AT2023hkw, and AT2023vth. As with the stellar mass differences, this also due to our implementation of a non-parametric SFH. While the cause of these differences in stellar mass and SFR is easily explained by our usage varying stellar population modeling methods, we emphasize the importance of using stellar population models with the same underlying physics to derive host properties for a given sample, as achieved here.

## 5. LFBOT LOCATIONS

In the following section, we determine basic properties of the LFBOT local environments, including their galactocentric offsets (physical and host-normalized) and how bright the host galaxy is at the transient’s location relative to the rest of the galaxy (fractional flux measurement). To contextualize these results, we furthermore compare their offset and fractional flux measurements to other transient populations. In Section 5.1, we discuss offsets and in Section 5.2, we measure and analyze their fractional flux.

### 5.1. Galactocentric Offsets

To determine the location of our LFBOT sample within their host galaxies, we begin by collecting the localizations of their Zwicky Transient Facility (ZTF; Bellm et al. 2019) detections from ALerCE (Automatic Learning for the Rapid Classification of Events). At the time of writing, there was no entry for AT2024wpp on ALerCE; thus, for this event, we instead collect localizations from the discovery bots listed on the Transient Name Server (TNS). Using the collected localizations, for each LFBOT we determine a median R.A. and Decl. and the  $1\sigma$  uncertainty on the localization. For CSS161010 (discovered prior to the start of ZTF), we simply use the localization and uncertainty determined in Coppejans et al. (2020) through radio observations of the transient. We list all localizations and positional uncertainties ( $\sigma_{\text{pos}}$ ) in Table 3.

**Table 3.** LFBOT Localizations

LFBOT	R.A.	Decl.	$\sigma_{\text{pos}}$ (arcsec)	$z$	$R_{\text{phys}}$ (kpc)	$R_{\text{hnorm}}$ ( $r/r_e$ )	Fractional Flux
AT2018cow	16 <sup>h</sup> 16 <sup>m</sup> 00.22 <sup>s</sup>	+22 <sup>d</sup> 16 <sup>m</sup> 04.89 <sup>s</sup>	0.328	0.0141	1.758±0.095	0.86 ± 0.05	0.67 <sup>+0.04</sup> <sub>-0.05</sub>
CSS161010	04 <sup>h</sup> 58 <sup>m</sup> 34.40 <sup>s</sup>	-08 <sup>d</sup> 18 <sup>m</sup> 03.95 <sup>s</sup>	0.03	0.033	0.258±0.02	0.49 ± 0.04	0.52 <sup>+0.0</sup> <sub>-0.0</sub>
ZTF18abvkw1	02 <sup>h</sup> 00 <sup>m</sup> 15.20 <sup>s</sup>	+16 <sup>d</sup> 47 <sup>m</sup> 57.32 <sup>s</sup>	0.147	0.272	2.401±0.619	1.11 ± 0.29	0.78 <sup>+0.02</sup> <sub>-0.3</sub>
AT2020mrf	15 <sup>h</sup> 47 <sup>m</sup> 54.17 <sup>s</sup>	+44 <sup>d</sup> 39 <sup>m</sup> 07.41 <sup>s</sup>	0.12	0.1353	1.242±0.291	0.9 ± 0.21	0.75 <sup>+0.09</sup> <sub>-0.2</sub>
AT2020xnd	22 <sup>h</sup> 20 <sup>m</sup> 02.02 <sup>s</sup>	-2 <sup>d</sup> 50 <sup>m</sup> 25.38 <sup>s</sup>	0.235	0.243	1.071±0.911	0.46 ± 0.43	0
AT2022tsd	03 <sup>h</sup> 20 <sup>m</sup> 10.86 <sup>s</sup>	+08 <sup>d</sup> 44 <sup>m</sup> 55.96 <sup>s</sup>	0.095	0.256	6.106±0.382	1.67 ± 0.1	0.24 <sup>+0.12</sup> <sub>-0.23</sub>
AT2023fhn	10 <sup>h</sup> 08 <sup>m</sup> 03.82 <sup>s</sup>	+21 <sup>d</sup> 04 <sup>m</sup> 26.89 <sup>s</sup>	0.132	0.238	17.400±0.503	2.42 ± 0.07	0
AT2023hkw	10 <sup>h</sup> 42 <sup>m</sup> 17.73 <sup>s</sup>	+52 <sup>d</sup> 29 <sup>m</sup> 18.99 <sup>s</sup>	0.394	0.335	13.58±1.92	1.91 ± 0.27	0.0 <sup>+0.06</sup> <sub>-0.0</sub>
AT2023vth	17 <sup>h</sup> 56 <sup>m</sup> 34.40 <sup>s</sup>	+08 <sup>d</sup> 02 <sup>m</sup> 37.37 <sup>s</sup>	0.048	0.0747	2.86±0.07	1.91 ± 0.27	0.51 <sup>+0.0</sup> <sub>-0.0</sub>
AT2024qfm	23 <sup>h</sup> 21 <sup>m</sup> 23.46 <sup>s</sup>	+11 <sup>d</sup> 56 <sup>m</sup> 32.03 <sup>s</sup>	0.272	0.227	4.078±1.001	1.6 ± 0.4	0.0 <sup>+0.23</sup> <sub>-0.0</sub>
AT2024wpp	02 <sup>h</sup> 42 <sup>m</sup> 05.483 <sup>s</sup>	-16 <sup>d</sup> 57 <sup>m</sup> 22.98 <sup>s</sup>	0.206	0.0866	5.987±0.338	0.97 ± 0.06	0.34 <sup>+0.09</sup> <sub>-0.13</sub>

NOTE—The localizations, localization uncertainties ( $\sigma_{\text{pos}}$ ), redshifts, physical galactocentric offsets  $R_{\text{phys}}$ , host-normalized offsets ( $R_{\text{hnorm}}$ ), and fractional flux for our LFBOT sample. The localization for CSS161010 was determined in Coppejans et al. (2020) and the localization for AT2024wpp was determined with data available on TNS. All other localizations were determined from the listed ZTF detections of each LFBOT on ALeRCE.

We determine physical galactocentric offsets ( $R_{\text{phys}}$ ) by measuring the distance of the transient location to the center of their respective host (determined through our photometric techniques or listed in other works; Table A1), propagating the LFBOT localization uncertainty into the offset uncertainty. We furthermore determine a host-normalized offset:  $R_{\text{hnorm}} = r/r_e$ , where  $r$  is the angular galactocentric offset of the LFBOT and  $r_e$  is the half-light radius of the host galaxy. We collect  $r_e$  measurements (and uncertainties) for all LFBOT hosts from DECaLS, except for the hosts of AT2020mrf, AT2022tsd, and AT2023vth where one was not measured. Instead, we employ `SEP.flux_radius` routine over the  $g$ -band Hyper Suprime-Cam Subaru Strategic Program (HSC-SSP; Aihara et al. 2018, 2019) image for AT2020mrf, Keck/LRIS  $G$ -band image for AT2022tsd, and PanSTARRS  $g$ -band image for AT2023vth to determine the radius where half the host galaxy flux is constrained. Unlike DECaLS, `SEP` does not provide an uncertainty for the  $r_e$ ; thus we adopt an uncertainty of 1% the measured  $r_e$ , which is roughly consistent with the errors obtained for the other hosts. To determine uncertainty on  $R_{\text{hnorm}}$ , we randomly sample 10,000  $r$  and  $r_e$  values, using their median and  $1\sigma$  uncertainties, to generate 10,000  $R_{\text{hnorm}}$  values. We list the median and  $1\sigma$  uncertainty of  $R_{\text{phys}}$  and  $R_{\text{hnorm}}$  in Table 3 for our LFBOT sample.

In Figure 6, we present the LFBOT  $R_{\text{phys}}$  and  $R_{\text{hnorm}}$  CDFs and 68% interval on each CDF. To properly account for uncertainty on both offset CDFs, we randomly sample 10,000 offsets for each LFBOT from a

Rice Distribution using their median offset and  $1\sigma$  uncertainty, following the methods outlined in Blanchard et al. (2016). The Rice distribution guarantees that the sampled offset is a positive integer value (mitigating the effect large uncertainties can have on the sampled value). We note that that when  $R/\sigma R > 5$ , the Rice distribution reduces to a Gaussian distribution.

We find that LFBOTs have  $R_{\text{phys}} = 2.89^{+9.36}_{-1.71}$  kpc (population median and 68% interval) and  $R_{\text{hnorm}} = 1.19^{+0.72}_{-0.49} r/r_e$ . To place these results in the context of other transient populations, we compare them to the  $R_{\text{phys}}$  and  $R_{\text{norm}}$  distributions of SNe II, SNe Ibc, SNe Ibn, SLSNe-I, and LGRBs. We collect offset distributions for SNe II and Ibc in Prieto et al. (2008), SNe Ibn in Dong et al. (2025), SLSNe-I in Hsu et al. (2024), and LGRBs in Blanchard et al. (2016) and showcase CDFs of these distributions also in Figure 6. Qualitatively, it appears that the LFBOTs have a similar  $R_{\text{phys}}$  distribution to those of SNe II, Ibc, and Ibn, but trace higher  $R_{\text{phys}}$  than SLSNe-I and LGRBs. To quantitatively assess this, we perform 10,000 AD tests between a single realization of the LFBOT  $R_{\text{phys}}$  CDF and that of the transient of interest and reject the null hypothesis that the transient and LFBOT derive from the same underlying offset distributions when  $> 50\%$  of  $p_{AD} < 0.05$ . We are not able to reject the null hypothesis when comparing the LFBOT  $R_{\text{phys}}$  distribution to SNe II, Ibc, and Ibn (0%, 0.2%, and 0% of  $p_{AD} < 0.05$ , respectively). We confirm that LFBOTs do indeed trace higher  $R_{\text{phys}}$  than SLSNe-I and LGRBs, given that 100% of  $p_{AD} < 0.05$  when comparing LFBOTs to each transient sample.

Unlike the other transient populations, there appears to be a lack of LFBOTs that occur at low  $R_{\text{hnorm}}$ . In-

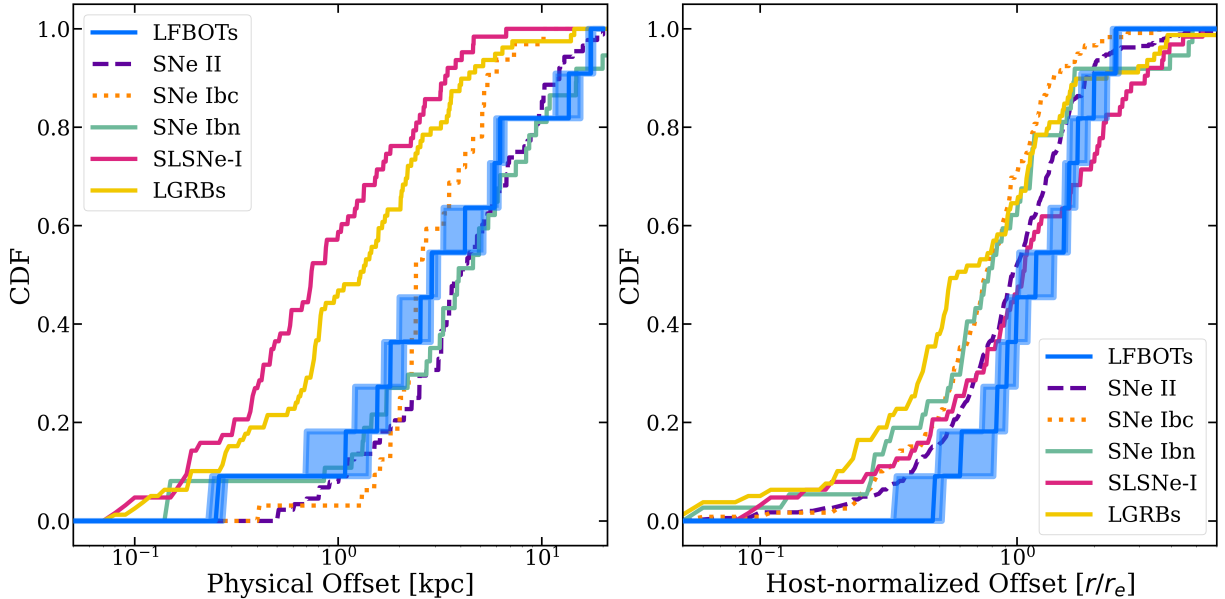


**Figure 6.** The physical galactocentric offset (*left*) and host-normalized offset (*right*) distributions of LFBOTs (blue; median and 68% interval) compared to those of SNe II (purple dashed line), Ibc (orange dotted line), Ibn (green), SLSNe-I (pink), and LGRBs (yellow). LFBOTs have similar physical offset distributions to SNe II, Ibc, and Ibn and are more offset than SLSNe-I and LGRBs. Additionally, LFBOTs have larger host-normalized offsets than LGRBs, SNe Ibc, and SN Ibn and more similar distributions to SNe II and SLSNe-I.

deed, visually, it seems that the LFBOT  $R_{\text{hnorm}}$  distribution skews towards higher offsets than SLSNe-I, LGRBs, SNe Ibc, and Ibn. When comparing these distributions with AD tests, we do find that LFBOTs trace statistically different  $R_{\text{hnorm}}$  distributions than LGRBs (75% of  $p_{AD} < 0.05$ ), SNe Ibc (93% of  $p_{AD} < 0.05$ ), and SNe Ibn (93% of  $p_{AD} < 0.05$ ). This strongly suggests LFBOTs occur at higher  $R_{\text{hnorm}}$  than these transient populations. We do not, however, find that LFBOT  $R_{\text{hnorm}}$  distributions are statistically distinct from those of SNe II and SLSNe-I, as 0% of  $p_{AD} < 0.05$  in both cases.

Overall, while we do find that we can rule out similarities between offset distributions of LFBOTs and transients with likely massive star progenitors, LFBOTs do not appear to be extremely unique in comparison to these populations. Moreover, their  $R_{\text{phys}}$  and  $R_{\text{hnorm}}$  distributions lean toward significantly lower offsets than observed for short GRBs (Fong et al. 2022) and SNe Ia (Prieto et al. 2008; Wang et al. 2013): transients that derive from progenitors with long formation timescales (neutron star mergers and white dwarfs, respectively; Maoz et al. 2014; Abbott et al. 2017; Goldstein et al. 2017) and large systemic velocities that allow them to migrate far from their hosts’ centers (Zevin et al. 2020; Mandhai et al. 2022; Gaspari et al. 2024; Pan et al. 2026). Thus, from offset distribution alone, LFBOTs are much more aligned with transients from core-collapse

events and shorter formation timescales. We discuss implications for this result in Section 6.

## 5.2. Fractional Flux

Another useful statistic for characterizing the LFBOT local environment is determining its fractional flux. As originally described in Fruchter et al. (2006), fractional flux is defined as the sum of the flux of all the pixels fainter than those at the transient location divided by the total host galaxy flux. In turn, we obtain a measurement for how bright the galaxy is at the location of the transient, where a fractional flux of 0 is the faintest pixel within the host (or the transient lies outside the host galaxy’s light) and 1 is the brightest pixel. In star-forming galaxies, we may expect that young, massive stellar populations will trace the brightest regions of their host.

We follow the methodology in Hsu et al. (2024) to determine the fractional flux and quantify its uncertainty for each LFBOT in our sample. For each LFBOT, we use the highest quality, bluest optical filter (preferring  $g$ -band since all LFBOTs have  $g$ -band observations) to perform the fractional flux calculation. Bluer filters specifically help us probe recent star formation in the hosts. We use the  $g$ -band image listed in Table A1 for AT2020mrf, AT2022tsd, AT2023vth, and AT2024wpp. For AT2020xnd and AT2023fhn, we use the  $r$  and  $V$ -band images as these are the highest quality, bluest images for both of these transients. Finally, we download

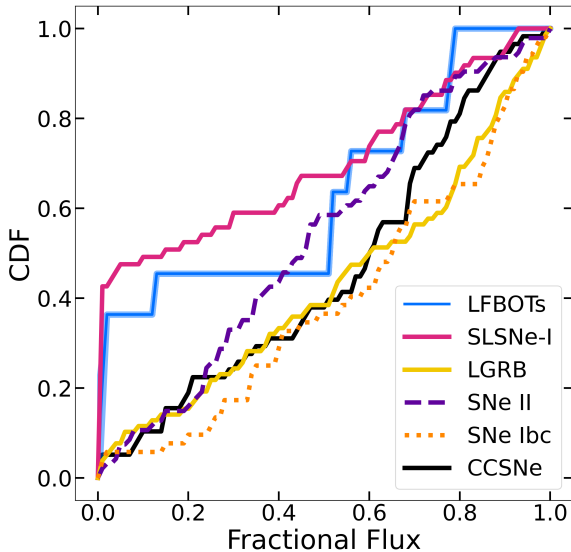


**Figure 7.** The fractional flux distributions of LFBOTs (blue; median and 68% interval) compared to those of SNe II (purple dashed line), Ibc (orange dotted line), SLSNe-I (pink), and LGRBs (yellow). Similar to SLSNe, a large fraction of LFBOTs occur in the faintest region of their host galaxy or outside their host galaxy’s light and they clearly trend towards lower fractional fluxes than LGRBs and the CCSNe populations.

DECaLS  $g$ -band images via `FrankenBlast` for the hosts of AT2018cow, CSS161010, ZTF18abvkw1, AT2023hkw, and AT2024qfm. We determine an uncalibrated total host flux in a similar manner as described in Section 2.1 with `SEP`. Here, however, we measure a Kron radius using a threshold of  $1\sigma$  above sky background to ensure that we extract all potential faint pixels on the outskirts of the galaxy.

As done in [Hsu et al. \(2024\)](#), we use a Monte Carlo routine to determine the pixels that overlap with each LFBOT location, which we propagate into the fractional flux uncertainty. We sample 10,000  $(x, y)$  pixel coordinates from a 2D Gaussian distribution, assuming the pixel at the median transient localization (Table 3; Section 5.1) is the centroid of the Gaussian and  $\sigma_{\text{pos}}$  is the standard deviation. We calculate a fractional flux for each pixel and report the median and 68% interval for each LFBOT in Table 3. We note that two LFBOTs (AT2020xnd and AT2023fhn) lie outside their host galaxy’s Kron radius and thus they have a fractional flux of 0.

We use the 10,000 fractional flux samples for each LFBOT to build 10,000 realization on the CDF, and highlight the median and 68% interval on the CDF in Figure 7 (we note that uncertainties on the fractional flux

are small, hence why the width of the CDF is also small). We contextualize these results by comparing them to fractional flux distributions of SLSNe-I (from [Hsu et al. 2024](#)), LGRBs (from [Blanchard et al. 2016](#)), and SNe II and Ibc (from [Kelly et al. 2008](#)). We also include the general CCSNe fractional flux distribution from [Svensson et al. \(2010\)](#).

From visual examination, it appears that LFBOTs trace a more similar fractional flux distribution to SLSNe-I than the other transient populations. While CCSNe and LGRBs have very few (if any) events with 0 fractional flux, both LFBOTs and SLSNe-I have a high fraction events ( $> 30\%$ ) at their hosts faintest pixel or beyond their host’s light radius and generally appear to trace lower fractional fluxes than CCSNe. When comparing the distributions with AD tests (performed in the same way as for offsets), we confirm these qualitative assessments. We find that we are not able to reject the null hypothesis that LFBOTs and SLSNe trace the same underlying fractional flux distribution, as 0% of  $p_{AD} < 0.05$ . Meanwhile, we find that we can reject the null hypothesis for the LFBOT fractional flux distribution compared to LGRBs, SNe II, and SNe Ibc as 94%, 54%, and 97% of  $p_{AD} < 0.05$ , respectively. We furthermore determine that LFBOTs trace statistically different fractional flux distributions than the general CCSNe population (71% of  $p_{AD} < 0.05$ ). Thus, we conclude that LFBOTs, like SLSNe-I, generally occur in fainter pixels in their hosts, or outside of their hosts’ light, than CCSNe. We discuss these results in the context of possible progenitor systems in Section 6.

## 6. DISCUSSION

In this section, we analyze LFBOT host stellar populations, galactocentric offset and fractional flux distributions to test the viability of various progenitor scenarios. Our goal is to determine whether proposed models such as TDEs, failed SNe, PPISNe, magnetar-powered SN, or compact object-WR mergers are physically consistent with our findings. Although LFBOTs may arise from multiple formation pathways, here we evaluate whether their environmental properties can be explained by a single progenitor channel. Finally, we emphasize that the population of LFBOTs and their hosts is currently quite small, thus it is possible that any inferences we make may change with a larger population. Nonetheless, we do find consistencies within the current LFBOT sample from which we can begin to constrain their progenitors. We organize this section by discussing each progenitor model in the context of our findings.

### 6.1. IMBH TDE?

A TDE origin for LFBOTs was originally proposed, motivated by the prototypical event AT2018cow, which showed a steep lightcurve decline, blue and featureless spectrum, and late-time He emission reminiscent of the tidal disruption of stars by SMBHs (Kuin et al. 2019; Perley et al. 2019). Unlike SMBH TDEs, LFBOT lightcurves initially rise and decay on  $\approx$ days timescales rather than weeks to months, which would require a less massive black hole, similar to that of IMBHs ( $10^3 - 10^6 M_\odot$ ), to power the transient (Perley et al. 2019; Winter-Granic & Quataert 2025). Early LFBOT host galaxy analyses also supported an IMBH TDE origin, as the first discovered LFBOTs were all associated with dwarf galaxies (AT2018cow, CSS161010, ZTF18abvkw1, AT2020mrf, and AT2020xnd; Perley et al. 2019, 2021; Ho et al. 2020; Yao et al. 2022), for which a central mass BH would plausibly be in the IMBH mass range. Here, we find several properties of LFBOTs and their hosts that disfavor this progenitor model. For one, while LFBOT hosts do lean towards lower mass galaxies, they are not all strictly dwarf galaxies ( $< 10^9 M_\odot$ ). Thus, we can assume that the central BH stellar mass likely spans a large range, from IMBH to SMBH ( $> 10^6 M_\odot$ ) masses. Moreover, as we show in Section 5.1, LFBOTs are not centrally located within their hosts. Rather, it appears that LFBOTs have a lack of events at low physical and host-normalized offsets, especially in comparison to CC-SNe, LGRBs, SLSNe-I, and SNe Ibn. Therefore, we find no reason to believe that LFBOTs represent interactions with or accretion onto a central massive BH.

We next consider whether LFBOTs are powered by a TDE from a wandering IMBH, which we would expect to occur in off-nuclear locations and not exclusively in dwarf galaxy environments. Recently, observational evidence has emerged for TDEs created from BHs “wandering” from their hosts, based on the discovery of four off-nuclear TDEs with likely BH masses  $> 10^4 M_\odot$  (Guolo et al. 2026; Guolo 2026; Stein et al. 2026). Although it may seem more promising that LFBOTs arise from this IMBH TDE channel, we still disfavor this scenario. Wandering IMBHs likely form through the capture of the central BHs of interacting dwarf galaxy satellites by the larger primary galaxy (Bellovary et al. 2010; Greene et al. 2021; Ricarte et al. 2021). As galaxies grow hierarchically through mergers, larger galaxies have generally experienced more mergers and thereby should host more wandering IMBHs. Indeed, Guolo (2026) predict that the number of wandering IMBHs, and thus the probability of off-nuclear TDEs, increases with host stellar mass. This is further supported by the properties of the current population off-nuclear TDE hosts, as all are elliptical galaxies with large stellar masses, rang-

ing  $10.7 \lesssim \log(M_*/M_\odot) \lesssim 11.2$  (Guolo 2026). Given that LFBOTs exclusively occur in star-forming galaxies with a much lower stellar masses, we find it improbable that they originate through a wandering IMBH channel. Thus, even with a small population of LFBOTs, we find significant evidence to suggest they do not derive from IMBH TDEs.

The IMBH TDE model is also in tension with other observed LFBOT properties. Specifically, LFBOTs are surrounded by a dense, extended CSM, inferred from their radio emission, which is difficult to justify in an IMBH TDE scenario (Ho et al. 2019, 2020, 2022; Margutti et al. 2019; Coppejans et al. 2020; Bright et al. 2022; Yao et al. 2022; Chrimes et al. 2024a,b; Nayana et al. 2025; Sevilla et al. 2026). Given the lack of support of the IMBH TDE model from both the transient and host properties, we strongly disfavor this progenitor theory for LFBOTs.

## 6.2. Stellar Mass Compact Object TDE?

We next turn our attention to the stellar mass compact object TDE progenitor channel discussed in Tsuna & Lu (2025). In this scenario, a massive star in a tight field binary undergoes a CCSN, forming a remnant NS or BH. The natal kick imparted on the compact object leads to a chance collision with a (typically, main-sequence) stellar companion, which is then tidally disrupted and accreted by the compact object. Tsuna & Lu (2025) predict that the transient emission from this event will reach the peak luminosities observed for LFBOTs, with similarly rapid lightcurve evolution when modeling scenarios with low ejecta masses. In addition, their model predicts late-time H emission ( $\approx 20$  days post-peak, similar to AT2018cow; Prentice et al. 2018; Perley et al. 2019) observed in some LFBOTs, which is difficult to reproduce in other progenitor scenarios. This late-time emission arises from CCSN ejecta becoming optically thin, allowing detection of H lines from the disrupted companion star.

Our findings on LFBOT environments are also in tension with this progenitor model. First, from our analysis on LFBOT fractional fluxes, we find clear evidence that the LFBOT progenitor has been forced out of the star-forming region within its host and birthsite. This is likely caused by either massive star that has received a significant kick or a progenitor with a longer formation timescale than a core-collapse event. This BH/NS TDE model satisfies neither of these scenarios, given that the TDE occurs almost immediately ( $\approx$  weeks) after the first star undergoes core-collapse: an insignificant amount of time for the binary to migrate away from its these regions. Moreover, to the extent that most massive stars

are in binaries at birth, there is nothing particularly different about this progenitor set-up than normal CCSN models, except that a chance kick from the SN happened leads to immediate merger. Therefore, if LFBOTs were to arise from this channel, their environments should largely be similar those of the normal CCSN population. Here, we clearly show that LFBOT hosts are quite distinct from CCSN hosts in both metallicity and star formation, which disfavors most LFBOTs being connected to this progenitor channel.

### 6.3. *Stellar Death or Supernovae?*

An alternative progenitor theory postulates that LFBOTs arise from stellar deaths, with possible origins including PPISNe (Leung et al. 2020), failed SNe (Margutti et al. 2019; Perley et al. 2019; Quataert et al. 2019; Antoni & Quataert 2022), and magnetar-powered SNe (Prentice et al. 2018; Vurm & Metzger 2021). Central to each of these scenarios is the formation of a compact object that is either rapidly-rotating or accreting at super-Eddington rates to heat the supernova ejecta and power the LFBOT lightcurve. The classification of many lower-luminosity FBOTs (Drout et al. 2014) as CCSNe (Ho et al. 2023b) highlight a possible connection between LFBOTs and the deaths of massive stars. From LFBOT host properties, we find some evidence that they may originate from the final stages of massive star evolution, which we explore below.

#### 6.3.1. *PPISNe?*

Within our sample, we observe that LFBOTs tend to occur in actively star-forming galaxies with recent bursts of star formation and low metallicities: the perfect environment for massive star formation. This preference could hint that LFBOTs represent a massive core-collapse event, or, at the very least, have a young, massive stellar component in their progenitor system. Under the assumption that LFBOTs originate from stellar deaths of massive stars, their comparisons to the environments of SLSNe-I, LGRBs, and CCSNe does impose some constraints on the nature of their progenitor. For one, we show that LFBOTs occur in more metal-poor environments than SNe Ibc and SNe II, whose progenitors are thought to be stripped-envelope WR stars and red supergiants (RSGs), respectively (Smartt et al. 2009; Smith et al. 2011; Smith 2014; Smartt 2015). At face value, this may suggest that the LFBOT progenitors are more massive stars, which more easily form at low metallicities. However, we also find that LFBOT hosts are neither as metal-poor nor as intensely star-forming as those of SLSNe-I and LGRBs. Both of these transients are thought to derive from the core-collapse of very massive, highly metallicity-dependent stars (e.g.,

Heger et al. 2003; Woosley & Bloom 2006; Leloudas et al. 2015; Nicholl et al. 2017; Blanchard et al. 2020). Thus, we infer that while LFBOT progenitors may come from more massive stars than SNe Ibc and II, they are likely not as massive or metallicity-dependent as SLSNe-I and LGRB progenitors. We, therefore, strongly disfavor PPISNe as an LFBOT progenitor, as it is assumed that they originate from more massive and metal-poor stars than SLSNe-I and LGRBs (Heger et al. 2003; Woosley 2017) and would reside hosts with a stronger metallicity dependence than either population.

#### 6.3.2. *Failed SNe?*

On the other hand, the failed SN progenitor model could explain why LFBOTs have a stronger metallicity dependence than CCSNe, but weaker than SLSNe-I and LGRBs. In this scenario, a massive star (possibly a blue supergiant; Margutti et al. 2019) collapses into a BH after neutrino-induced mass loss and accretes the remaining stellar material, creating luminous emission (Lovegrove et al. 2017; Quataert et al. 2019; Antoni & Quataert 2022). It is thought that high angular momentum of the progenitor star is crucial in forming the accretion disk, although this has been debated (Quataert et al. 2019). Metallicity is thought to play a large role in the intrinsic angular momentum of stars, since at higher metallicity, stars will lose angular momentum due to mass loss from metal-driven winds (Heger et al. 2003). There is indeed observational support for this, as metal-driven mass loss likely leads to the formation of more stripped-envelope SNe Ibc, which are found in more metal-rich hosts than SNe II (Prieto et al. 2008; Anderson et al. 2010; Modjaz et al. 2011; Kelly & Kirshner 2012; Galbany et al. 2016; Schulze et al. 2021; Qin & Zabludoff 2024). Thus, we would expect failed SN to preferentially occur in lower metallicity environments than at least SNe Ibc, which we do find for LFBOTs.

If LFBOTs are powered by failed SNe, however, it is not clear why their fractional flux distribution significantly deviates from that of CCSNe. The high fraction of LFBOTs at zero fractional flux signals that their progenitor has been ejected from their birthsite and is traveling at high systemic velocities (higher than assumed for CCSN). Yet, it is unclear why certain core-collapse events would receive much stronger kicks than others. A possible way to reconcile these differences is if the LFBOT failed SN progenitor is in a binary system, since binary interactions can displace SNe in their hosts (Blaauw 1961; Aghakhanloo et al. 2017; Renzo et al. 2019; Wagg et al. 2025). Binary interactions may also spin up stars, establishing the necessary conditions for a star to undergo a failed SN. However, considering

that most massive stars are in binary or multiple stellar systems (Chini et al. 2012; Sana et al. 2012; Dunstall et al. 2015; Moe & Di Stefano 2017), we can presume that a large number of SNe Ib/c and II are also influenced by binary physics. Consequently, to fully validate the failed SN scenario for LFBOTs, we must determine why this specific model would impart significantly larger natal kicks than those assumed for standard CCSNe.

### 6.3.3. Magnetar-powered SNe?

It was also suggested that LFBOTs originate from magnetar-powered SNe, in which a successful CCSNe produces a rapidly spinning, millisecond magnetar remnant (e.g., Prentice et al. 2018). In this case, the LFBOT lightcurve is powered by the magnetar spin-down that heats the SN ejecta, keeping the transient emission blue for an extended period. Interestingly, this is also the most prevailing progenitor theory for SLSNe-I (Kasen & Bildsten 2010; Leloudas et al. 2015; Metzger et al. 2015; Nicholl et al. 2015, 2017; Blanchard et al. 2020). Similar to LFBOTs, SLSNe-I have high peak luminosities and lightcurves that cannot be solely explained by  $^{56}\text{Ni}$  decay, suggesting they too have a central engine. However, SLSNe-I are generally much more slowly evolving transients than LFBOTs. The disparity can potentially be reconciled by progenitor mass; for instance, LFBOTs may involve less massive progenitors that produce lower ejecta masses than those of SLSNe-I (Margutti et al. 2019). Our environmental analysis clearly reveals that LFBOTs and SLSNe-I do not occur in similar host galaxies, as SLSNe-I hosts are more metal-poor, more star-forming, and less massive than LFBOT hosts. The only apparent similarity in SLSNe-I and LFBOT environments are their fractional flux distributions, where a large fraction of both transient populations occur in fainter regions of their hosts. Thus, nominally, the differences between their environments do not indicate that SLSNe-I and LFBOTs share the same progenitor.

A possible way to connect SLSNe-I and LFBOTs, assuming they both originate from magnetar-powered SNe, is by invoking binary versus solitary star progenitor channels. To form a millisecond magnetar, the progenitor star must have high angular momentum, which is either intrinsic to the star or achieved through a binary companion. As just discussed in the case of failed SNe, retaining high angular momentum throughout a stellar lifetime can be a natural consequence of low metallicity. On the other hand, low metallicity is not a strict requirement for a star that inherits angular momentum through its binary companion. With this in mind, we may infer that SLSNe-I originate from a single star channel, as

they do occur in lower metallicity environments, whereas the LFBOT progenitor is in a binary system. Yet, this dichotomy breaks down when considering the local environments of these transients. The fractional flux distributions of both SLSNe-I and LFBOTs highlight that both of their progenitors have received a kick to migrate away from star-forming regions within their hosts, which is incommensurate with a solitary star channel, but a possible outcome in the binary scenario. Indeed, Hsu et al. (2024) speculates that SLSNe-I arise from a disrupted binary system to achieve estimated systemic velocities on the order of  $100 \text{ km s}^{-1}$ . Thus, while we don't completely rule out the possibility that LFBOTs represent a millisecond magnetar channel, we struggle to rationalize this progenitor scenario if SLSNe-I are indeed magnetar-powered SNe. Finally, there is also some question as to whether the millisecond magnetar channel can produce the dense, extended CSM and asymmetric ejecta observed in several LFBOTs (Margutti et al. 2019; Vurm & Metzger 2021; Metzger 2022) or the large accretion disk inferred by modeling the late time UV and X-ray spectrum (Chen et al. 2023; Migliori et al. 2024; Inkenhaag et al. 2025; Winter-Granic & Quataert 2025).

### 6.4. Compact Object and Wolf-Rayet Star Merger?

We lastly consider the possibility that LFBOTs arise from the merger between a stellar mass BH or NS and the evolved He core of a binary companion (WR star), which has been proposed in Metzger (2022) and Klencki & Metzger (2025). In this model, the merger is predicted to occur after a binary system, initially comprised of a compact object and main-sequence star, undergoes a common-envelope or stable mass transfer phase. During this phase, the Hydrogen envelope of the star is accreted by the compact object, tightening the binary and leading to a BH/NS-WR star pair. The system eventually merges due to angular momentum loss, causing the compact object to tidally disrupt the WR star. Luminous transient emission is produced from accretion of the stellar material at super-Eddington rates and shocks with the CSM, created from the earlier WR star mass-loss episode. Since explosive nucleosynthesis is minimal, this merger model is also consistent with the low  $^{56}\text{Ni}$  yields inferred in LFBOTs (Metzger 2022; Neights et al. 2026).

Our findings on LFBOT environments are compatible with this progenitor scenario, especially in comparison to the aforementioned progenitor models. First, Klencki & Metzger (2025) determines that these mergers will preferentially occur in environments with subsolar, but not extremely low, metallicities, given that (i) massive

compact objects more easily form at low metallicities, and (ii) binary interactions with a WR star are more frequent at low metallicity (Klencki et al. 2020). Thus, this model naturally explains the slight low-metallicity bias we find in the LFBOT host population. It is furthermore expected that there will be a delay ( $\approx$ few Myr) between formation of the compact object (via CCSNe) and the merger. This allows enough time for the natal kick from the SN to propel the system to the outskirts of the host galaxy and provides clear rationale for the observed LFBOT fractional flux distribution. Lastly, the total time delay between the birth of the binary system until the merger will is not so long ( $\approx$  tens of Myr) that we would expect their hosts to evolve significantly off the SFMS or grow substantially in stellar mass. In turn, we would expect these mergers to favor actively star-forming hosts, possibly with recent bursts of star formation in which the binary was formed, that are not exceptionally massive: exactly what we currently observe with the LFBOT host population.

It is further interesting to note that Metzger (2022) predicts that some SNe Ibn/Icn may also come from this same progenitor channel. Specifically, they hypothesize that these SNe originate from systems with longer delays (by  $\sim 10^3 - 10^5$  yr) between the first common-envelope phase and the merger than assumed for the LFBOT channel. Our results may indicate a common origin between LFBOTs and SNe Ibn, though, we note both of their host populations are small and thus any observed similarity will be influenced by small-number statistics. We show that SNe Ibn occur in hosts that are slightly less star-forming, but have similar metallicities to LFBOT hosts. From the similar metallicity dependence of both transient classes, we may infer that the LFBOT and SN Ibn arise from similar stellar progenitors. The slight difference in star-formation activity in their hosts may solely be an indication of the longer delay times of the SNe Ibn progenitor channel, where we would expect the hosts to be more evolved. While no fractional flux distribution currently exists for SNe Ibn, several events occur well outside host galaxy’s light (Hosseinzadeh et al. 2019; Dong et al. 2025), including one event within the small but growing population of SNe Icn (Aster et al. 2026; Hu et al. 2026; Shi et al. 2026). This suggests, similar to LFBOTs, that their progenitors have been impacted by kicks that eject them from their birthsite. Future studies on SNe Ibn/Icn and their environments should explore their similarity to LFBOT hosts and determine if there is indeed a shared progenitor channel.

A potential caveat to the BH/NS-WR star merger progenitor scenario for LFBOTs is that a similar progeni-

tor system was proposed to power ultra-long GRB jet ( $\approx 10^3 - 10^5$  s) during the merger (Fryer & Woosley 1998; Zhang & Fryer 2001; Klencki & Metzger 2025), though perhaps only in the subset of events in which the BH is rapidly spinning. On-axis GRB jets have been confidently ruled-out within the current population of LFBOTs (Margutti et al. 2019; Coppejans et al. 2020; Ho et al. 2020; Yao et al. 2022; Ho et al. 2023a; Nayana et al. 2025). However, it remains plausible for several events to be associated with (undetected) off-axis GRB jets (Margutti et al. 2019; Ho et al. 2020, 2023a; Nayana et al. 2025). If GRB jets do precede LFBOTs, it would intrinsically connect them to the population of long and ultra-long GRBs. Typical LGRBs are thought to arise from massive collapsar events, in which a massive, rapidly rotating star collapses into a BH, forming an accretion disk that powers the relativistic jet (Woosley 1993). To gain enough angular momentum to create the accretion disk, several studies advocate that the LGRB progenitor must be in a tight binary system (Fryer et al. 1999, 2025), including a BH/NS-WR star system. Alternatively, Fryer & Woosley (1998) and Zhang & Fryer (2001) suggest that a BH-WR star merger, with a similar formation channel as discussed in Metzger (2022), could be responsible for some LGRBs. This, furthermore, was the proposed progenitor model for ultra-long GRBs 101225A (Thöne et al. 2011) and 250702B (Neights et al. 2026). Notably, ultra-long GRBs are also expected to have lower  $^{56}\text{Ni}$  yields than typical long GRBs (or, rather, the SNe Ic-BL following the long GRB), which does match the expectations for LFBOTs (Neights et al. 2026). While we do compare LFBOTs to LGRBs, we note that the population of ultra-long GRBs and their hosts is too small for a meaningful comparison. Lastly, no study has yet determined if LFBOT emission contributes to long or ultra-long GRB lightcurves.

If LGRBs and LFBOTs arise from similar tight binary evolutionary pathways, this may be hinted at in their environments. Here, we show that LFBOTs occur in more metal-rich hosts, have higher galactocentric offsets, and are associated with fainter regions of their hosts than LGRBs. In addition, it appears that LGRB hosts lie above the SFMS, whereas LFBOTs mostly track the SFMS (although we find no statistical difference between their 1D-sSFR and  $M_*$  distributions). The metallicity difference between LFBOTs and LGRBs, as well as the possible distinction between the hosts on the sSFR- $M_*$  plane is easily understood by the subtle differences in their progenitors. First, while it is not a requirement in the LFBOT merger progenitor scenario that the WR star is rapidly rotating, this is a re-

quirement with the LGRB scenario (whether they come from mergers or simply represent core-collapse events in tight binary systems). As such, the LGRBs should occur in lower-metallicity environments than LFBOTs, where the stellar companion can more easily retain high angular momentum. Moreover, if ultra-long GRBs precede at least some LFBOTs, as suggested in [Klencki & Metzger 2025](#), their progenitors should systematically arise from less massive stars than LGRBs, in either the merger or core-collapse scenario ([Zhang & Fryer 2001](#); [Fryer et al. 2025](#)). The formation of less massive compact objects and stellar companions inherently requires less of a metallicity-dependence than forming a more massive system.

The distinction between LGRB and LFBOT offsets and fractional fluxes may also be related to the total mass of the progenitor. More massive binaries likely travel with lower systemic velocities than less massive binaries. Furthermore, if we suppose that most LGRB progenitors undergo core-collapse before their tight-binary system can merge, they may also have slightly shorter formation timescales. Their progenitors thereby have a higher likelihood of staying closer to their birthsite, rather than getting kicked out as we see for LFBOTs. We believe that this comparison between LGRB and LFBOT hosts, although speculative on both of their progenitors, gives further support to the LFBOT BH/NS merger origin.

In total, we find the highest support for this compact object-WR star merger from LFBOT environments. All other progenitor models discussed have major caveats that contradict either the observed environmental properties of LFBOTs or their emission. While we don't completely rule out a stellar origin for LFBOTs, we implore future studies on LFBOTs and their progenitors to consider the effect that these models will have on their transients' observed fractional flux distribution, metallicity dependence, and comparison to other well-studied core-collapse events.

## 7. CONCLUSION

In this paper, we conducted an analysis of the environments of 11 LFBOTs, comprising the largest uniform analysis of LFBOT hosts to-date. To determine their host galaxy stellar population properties (stellar mass, amount of active star formation, metallicity, etc.), we modeled their host photometry and/or spectroscopy with *Prospector*. We additionally performed a simplistic analysis of LFBOT local environments by determining their physical and host-normalized galactocentric offset distributions and measuring their fractional fluxes. To contextualize these results, we compared

them to those derived for several CCSNe populations (SNe II, Ibc, and Ibn), LGRBs, and SLSNe-I: transients that LFBOTs have been frequently compared to in the literature. We list our main conclusions below:

- LFBOT hosts have  $\log(M_*/M_\odot) = 9.61^{+0.74}_{-1.61}$  (population median and 68% interval). LFBOT hosts have statistically similar stellar mass distributions to those of SN II, Ibc, Ibn, and LGRB hosts, but trace higher stellar masses than SLSNe-I.
- We determine that LFBOT hosts have present-day  $\text{SFR} = 0.95^{+18.37}_{-0.91} M_\odot \text{ yr}^{-1}$  and  $\log(\text{sSFR}) = -9.49^{+0.81}_{-0.66} \text{ yr}^{-1}$ . Compared to SLSN-I hosts, LFBOT hosts have lower sSFR. Meanwhile, they have higher sSFR than CCSN hosts and similar sSFR distributions to LGRB hosts.
- LFBOT hosts are all actively star-forming, but have a variety of SFH shapes. The majority of hosts are either currently in their most star-forming period or have had a star formation burst in the past  $\approx 100$  Myr.
- LFBOT hosts prefer SFR-weighted solutions in the 2D  $\text{SFR}-M_*$  plane, and possibly more SFR-weighted distributions than SNe Ibc and II hosts. They additionally occupy a different region in the 2D  $\text{SFR}-M_*$  plane than SLSNe-I and LGRBs, which appear to lean toward a higher-sSFR and lower- $M_*$  region than LFBOT hosts.
- LFBOT hosts have a gas-phase oxygen abundance  $12 + \log(\text{O}/\text{H}) = 8.71^{+0.17}_{-0.4}$ . This is lower metallicity than the general field galaxy population and CCSN hosts, but higher metallicity than SLSN-I and LGRB hosts.
- All LFBOT hosts lie in the star-forming galaxy phase space in the BPT diagrams, but have higher  $\log(\text{OIII}/\text{H}\beta)$  ratios in comparison to the general field galaxy population and CCSN hosts. These elevated ratios are also observed for LGRB and SLSN-I hosts and are likely caused by their hosts having low metallicities and high sSFRs.
- LFBOTs have physical galactocentric offsets  $= 2.89^{+9.36}_{-1.71}$  kpc and host-normalized galactocentric offsets  $1.19^{+0.72}_{-0.49} r/r_e$ . LFBOTs are more physically offset from their hosts than SLSNe-I and LGRBs but have similar physical offset distributions to CCSNe. In addition, they have larger host-normalized offsets than LGRBs, SNe Ibc, and SNe Ibn, but similar host-normalized offsets to SLSNe-I and SNe II.

- LFBOTs have a high fraction of events ( $> 30\%$ ) that occur in the faintest region of their host or outside of their hosts' light radii, which is similar to SLSNe-I, but distinct from LGRBs and CCSNe.

Our results indicate that the LFBOT progenitor includes a young, massive star, has a short formation timescale, and has received a large kick to eject it from star-forming regions within the host. Based on our finding, we strongly disfavor IMBH and stellar mass BH/NS TDEs progenitor channels for LFBOTs. While we are skeptical of stellar death and CCSN progenitor scenarios, we are not able to completely rule them out. In particular, we believe that there is a possibility that LFBOTs could comprise a failed SN or magnetar-powered CCSNe channel. However, the failed SN channel does not yet sufficiently explain the LFBOT fractional flux distribution. It is furthermore difficult to reconcile the magnetar-powered CCSNe channel if SLSNe-I also arise from the same progenitors, given the differences in their environments. We do find sufficient evidence that LFBOTs originate from the BH/NS-WR star mergers, which may connect the LFBOT progenitor to a variety of other astrophysical transients, including SNe Ibn/Icn, LGRBs, and ultra-long GRBs. A connection between their progenitors is also hinted at in their environments.

Our study establishes a crucial framework for constraining LFBOT progenitor channels through their host galaxy properties. We emphasize that the current sample of LFBOTs is quite small; as such, our findings should be viewed as a preliminary foundation for future population studies. Luckily, with the onset of the Vera C. Rubin Observatory's Legacy Survey of Space and Time (Rubin; [LSST Science Collaboration et al. 2009](#); [Ivezic et al. 2019](#)), we may soon achieve a statistically robust population of LFBOTs and their hosts. Indeed, given current LFBOT rate estimates ([Coppejans et al. 2020](#); [Ho et al. 2023b](#)), Rubin could discover tens to hundreds of LFBOTs each year. This large population will undoubtedly lend crucial insight into the breadth of LFBOT host properties, offsets, and their connection to recent star formation within their hosts. Moreover, with an increased sample sizes of all transients, we will better discern if LFBOTs share similar formation pathways to other events, including CCSNe, LGRBs, SLSNe-I, and SNe Ibn. Ultimately, the next few years promises to bring a much deeper understanding of these enigmatic, fascinating transients.

#### ACKNOWLEDGMENTS

We are grateful to Peter Blanchard, Lisa Kewley, Sarah Biddle, and Daichi Tsuna, who all provided extremely helpful guidance and suggestions on several

parts of this study. The Villar Astro Time Lab acknowledges support through the David and Lucile Packard Foundation, the Research Corporation for Scientific Advancement (through a Cottrell Fellowship), the National Science Foundation under AST-2433718, AST-2407922 and AST-2406110, as well as an Aramont Fellowship for Emerging Science Research. This work is supported by the National Science Foundation under Cooperative Agreement PHY-2019786 (the NSF AI Institute for Artificial Intelligence and Fundamental Interactions). BDM acknowledges support from NASA ATP (grant number 80NSSC22K0807), the Fermi Guest Investigator Program (grant number 80NSSC24K0408) and the Simons Foundation (grant number 727700). The Flatiron Institute is supported by the Simons Foundation. DF's contribution to this material is based upon work supported by the National Science Foundation under Award No. AST-2401779.

The computations in this paper were run on the FASRC Cannon cluster supported by the FAS Division of Science Research Computing Group at Harvard University.

This research has made use of the Keck Observatory Archive (KOA), which is operated by the W. M. Keck Observatory and the NASA Exoplanet Science Institute (NExSci), under contract with the National Aeronautics and Space Administration.

Based in part on data collected at the Subaru Telescope and retrieved from the HSC data archive system, which is operated by Subaru Telescope and Astronomy Data Center at National Astronomical Observatory of Japan. The Hyper Suprime-Cam (HSC) collaboration includes the astronomical communities of Japan and Taiwan, and Princeton University. The HSC instrumentation and software were developed by the National Astronomical Observatory of Japan (NAOJ), the Kavli Institute for the Physics and Mathematics of the Universe (Kavli IPMU), the University of Tokyo, the High Energy Accelerator Research Organization (KEK), the Academia Sinica Institute for Astronomy and Astrophysics in Taiwan (ASIAA), and Princeton University. Funding was contributed by the FIRST program from Japanese Cabinet Office, the Ministry of Education, Culture, Sports, Science and Technology (MEXT), the Japan Society for the Promotion of Science (JSPS), Japan Science and Technology Agency (JST), the Toray Science Foundation, NAOJ, Kavli IPMU, KEK, ASIAA, and Princeton University.

The Pan-STARRS1 Surveys (PS1) have been made possible through contributions of the Institute for Astronomy, the University of Hawaii, the Pan-STARRS Project Office, the Max-Planck Society and its par-

ticipating institutes, the Max Planck Institute for Astronomy, Heidelberg and the Max Planck Institute for Extraterrestrial Physics, Garching, The Johns Hopkins University, Durham University, the University of Edinburgh, Queen’s University Belfast, the Harvard-Smithsonian Center for Astrophysics, the Las Cumbres Observatory Global Telescope Network Incorporated, the National Central University of Taiwan, the Space Telescope Science Institute, the National Aeronautics and Space Administration under Grant No. NNX08AR22G issued through the Planetary Science Division of the NASA Science Mission Directorate, the National Science Foundation under Grant No. AST-1238877, the University of Maryland, and Eotvos Lorand University (ELTE) and the Los Alamos National Laboratory.

The Legacy Surveys consist of three individual and complementary projects: the Dark Energy Camera Legacy Survey (DECaLS; Proposal ID #2014B-0404; PIs: David Schlegel and Arjun Dey), the Beijing-Arizona Sky Survey (BASS; NAOJ Prop. ID #2015A-0801; PIs: Zhou Xu and Xiaohui Fan), and the Mayall z-band Legacy Survey (MzLS; Prop. ID #2016A-0453; PI: Arjun Dey). DECaLS, BASS and MzLS together include data obtained, respectively, at the Blanco telescope, Cerro Tololo Inter-American Observatory, NSF’s NOIRLab; the Bok telescope, Steward Observatory, University of Arizona; and the Mayall telescope, Kitt Peak National Observatory, NOIRLab. Pipeline processing and analyses of the data were supported by NOIRLab and the Lawrence Berkeley National Laboratory (LBNL). The Legacy Surveys project is honored to be permitted to conduct astronomical research on Iolkam Du’ag (Kitt Peak), a mountain with particular significance to the Tohono O’odham Nation.

NOIRLab is operated by the Association of Universities for Research in Astronomy (AURA) under a cooperative agreement with the National Science Foundation. LBNL is managed by the Regents of the University of California under contract to the U.S. Department of Energy.

This project used data obtained with the Dark Energy Camera (DECam), which was constructed by the Dark Energy Survey (DES) collaboration. Funding for the DES Projects has been provided by the U.S. Department of Energy, the U.S. National Science Foundation, the Ministry of Science and Education of Spain, the Science and Technology Facilities Council of the United Kingdom, the Higher Education Funding Council for England, the National Center for Supercomputing Applications at the University of Illinois at Urbana-Champaign, the Kavli Institute of Cosmological Physics

at the University of Chicago, Center for Cosmology and Astro-Particle Physics at the Ohio State University, the Mitchell Institute for Fundamental Physics and Astronomy at Texas A&M University, Financiadora de Estudos e Projetos, Fundacao Carlos Chagas Filho de Amparo, Financiadora de Estudos e Projetos, Fundacao Carlos Chagas Filho de Amparo a Pesquisa do Estado do Rio de Janeiro, Conselho Nacional de Desenvolvimento Cientifico e Tecnologico and the Ministerio da Ciencia, Tecnologia e Inovacao, the Deutsche Forschungsgemeinschaft and the Collaborating Institutions in the Dark Energy Survey. The Collaborating Institutions are Argonne National Laboratory, the University of California at Santa Cruz, the University of Cambridge, Centro de Investigaciones Energeticas, Medioambientales y Tecnologicas-Madrid, the University of Chicago, University College London, the DES-Brazil Consortium, the University of Edinburgh, the Eidgenossische Technische Hochschule (ETH) Zurich, Fermi National Accelerator Laboratory, the University of Illinois at Urbana-Champaign, the Institut de Ciencies de l’Espai (IEEC/CSIC), the Institut de Fisica d’Altes Energies, Lawrence Berkeley National Laboratory, the Ludwig Maximilians Universitat Munchen and the associated Excellence Cluster Universe, the University of Michigan, NSF’s NOIRLab, the University of Nottingham, the Ohio State University, the University of Pennsylvania, the University of Portsmouth, SLAC National Accelerator Laboratory, Stanford University, the University of Sussex, and Texas A&M University.

BASS is a key project of the Telescope Access Program (TAP), which has been funded by the National Astronomical Observatories of China, the Chinese Academy of Sciences (the Strategic Priority Research Program “The Emergence of Cosmological Structures” Grant # XDB09000000), and the Special Fund for Astronomy from the Ministry of Finance. The BASS is also supported by the External Cooperation Program of Chinese Academy of Sciences (Grant # 114A11KYSB20160057), and Chinese National Natural Science Foundation (Grant # 12120101003, # 11433005).

The Legacy Survey team makes use of data products from the Near-Earth Object Wide-field Infrared Survey Explorer (NEOWISE), which is a project of the Jet Propulsion Laboratory/California Institute of Technology. NEOWISE is funded by the National Aeronautics and Space Administration.

The Legacy Surveys imaging of the DESI footprint is supported by the Director, Office of Science, Office of High Energy Physics of the U.S. Department of Energy under Contract No. DE-AC02-05CH1123, by the

National Energy Research Scientific Computing Center, a DOE Office of Science User Facility under the same contract; and by the U.S. National Science Foundation, Division of Astronomical Sciences under Contract No. AST-0950945 to NOAO.

*Facilities:* Keck (LRIS); MMT (Binospec, MMIRS); VLT (FOR2)

*Software:* SEP (Barbary et al. 2016); POTPyRI (Paterson 2021); FrankenBlast (Nugent et al. 2026); PypeIt (Prochaska et al. 2020); Prospector (Johnson et al. 2021); FSPS and python-FSPS (Conroy et al. 2009; Conroy & Gunn 2010); dynesty (Speagle 2020)

## REFERENCES

- Abazajian, K. N., Adelman-McCarthy, J. K., Agüeros, M. A., et al. 2009, *ApJS*, 182, 543, doi: [10.1088/0067-0049/182/2/543](https://doi.org/10.1088/0067-0049/182/2/543)
- Abbott, B. P., Abbott, R., Abbott, T. D., et al. 2017, *ApJL*, 848, L13, doi: [10.3847/2041-8213/aa920c](https://doi.org/10.3847/2041-8213/aa920c)
- Aghakhanloo, M., Murphy, J. W., Smith, N., & Hložek, R. 2017, *MNRAS*, 472, 591, doi: [10.1093/mnras/stx2050](https://doi.org/10.1093/mnras/stx2050)
- Aihara, H., Arimoto, N., Armstrong, R., et al. 2018, *PASJ*, 70, S4, doi: [10.1093/pasj/psx066](https://doi.org/10.1093/pasj/psx066)
- Aihara, H., ALSayyad, Y., Ando, M., et al. 2019, *PASJ*, 71, 114, doi: [10.1093/pasj/psz103](https://doi.org/10.1093/pasj/psz103)
- Anderson, J. P., Covarrubias, R. A., James, P. A., Hamuy, M., & Haberman, S. M. 2010, *MNRAS*, 407, 2660, doi: [10.1111/j.1365-2966.2010.17118.x](https://doi.org/10.1111/j.1365-2966.2010.17118.x)
- Anderson, J. P., & James, P. A. 2009, *MNRAS*, 399, 559, doi: [10.1111/j.1365-2966.2009.15324.x](https://doi.org/10.1111/j.1365-2966.2009.15324.x)
- Angus, C. R., Levan, A. J., Perley, D. A., et al. 2016, *MNRAS*, 458, 84, doi: [10.1093/mnras/stw063](https://doi.org/10.1093/mnras/stw063)
- Antoni, A., & Quataert, E. 2022, *MNRAS*, 511, 176, doi: [10.1093/mnras/stab3776](https://doi.org/10.1093/mnras/stab3776)
- Arcavi, I., Gal-Yam, A., Kasliwal, M. M., et al. 2010, *ApJ*, 721, 777, doi: [10.1088/0004-637X/721/1/777](https://doi.org/10.1088/0004-637X/721/1/777)
- Aster, C., Inserra, C., Pastorello, A., et al. 2026, arXiv e-prints, arXiv:2602.20775, doi: [10.48550/arXiv.2602.20775](https://doi.org/10.48550/arXiv.2602.20775)
- Baldwin, J. A., Phillips, M. M., & Terlevich, R. 1981, *PASP*, 93, 5, doi: [10.1086/130766](https://doi.org/10.1086/130766)
- Barbary, K. 2016, *Journal of Open Source Software*, 1, 58, doi: [10.21105/joss.00058](https://doi.org/10.21105/joss.00058)
- Barbary, K., Boone, K., McCully, C., et al. 2016, *kbarbary/sep: v1.0.0, v1.0.0*, Zenodo, doi: [10.5281/zenodo.159035](https://doi.org/10.5281/zenodo.159035)
- Bellm, E. C., Kulkarni, S. R., Graham, M. J., et al. 2019, *PASP*, 131, 018002, doi: [10.1088/1538-3873/aaecbe](https://doi.org/10.1088/1538-3873/aaecbe)
- Bellovary, J. M., Governato, F., Quinn, T. R., et al. 2010, *ApJL*, 721, L148, doi: [10.1088/2041-8205/721/2/L148](https://doi.org/10.1088/2041-8205/721/2/L148)
- Bennett, C. L., Larson, D., Weiland, J. L., & Hinshaw, G. 2014, *ApJ*, 794, 135, doi: [10.1088/0004-637X/794/2/135](https://doi.org/10.1088/0004-637X/794/2/135)
- Bertin, E., & Arnouts, S. 1996, *A&AS*, 117, 393, doi: [10.1051/aas:1996164](https://doi.org/10.1051/aas:1996164)
- Blaauw, A. 1961, *BAN*, 15, 265
- Blanchard, P. K., Berger, E., & Fong, W.-f. 2016, *ApJ*, 817, 144, doi: [10.3847/0004-637X/817/2/144](https://doi.org/10.3847/0004-637X/817/2/144)
- Blanchard, P. K., Berger, E., Nicholl, M., & Villar, V. A. 2020, *ApJ*, 897, 114, doi: [10.3847/1538-4357/ab9638](https://doi.org/10.3847/1538-4357/ab9638)
- Bouquin, A. Y. K., Gil de Paz, A., Muñoz-Mateos, J. C., et al. 2018, *ApJS*, 234, 18, doi: [10.3847/1538-4365/aaa384](https://doi.org/10.3847/1538-4365/aaa384)
- Bradley, L., Sipőcz, B., Robitaille, T., et al. 2025, *astropy/photutils: 2.2.0, 2.2.0*, Zenodo, doi: [10.5281/zenodo.596036](https://doi.org/10.5281/zenodo.596036)
- Bright, J. S., Margutti, R., Matthews, D., et al. 2022, *ApJ*, 926, 112, doi: [10.3847/1538-4357/ac4506](https://doi.org/10.3847/1538-4357/ac4506)
- Brinchmann, J., Pettini, M., & Charlot, S. 2008, *MNRAS*, 385, 769, doi: [10.1111/j.1365-2966.2008.12914.x](https://doi.org/10.1111/j.1365-2966.2008.12914.x)
- Calzetti, D., Armus, L., Bohlin, R. C., et al. 2000, *ApJ*, 533, 682, doi: [10.1086/308692](https://doi.org/10.1086/308692)
- Cardelli, J. A., Clayton, G. C., & Mathis, J. S. 1989, *ApJ*, 345, 245, doi: [10.1086/167900](https://doi.org/10.1086/167900)
- Chabrier, G. 2003, *PASP*, 115, 763, doi: [10.1086/376392](https://doi.org/10.1086/376392)
- Chambers, K. C., Magnier, E. A., Metcalfe, N., et al. 2016, arXiv e-prints, arXiv:1612.05560, doi: [10.48550/arXiv.1612.05560](https://doi.org/10.48550/arXiv.1612.05560)
- Chen, T.-W., Smartt, S. J., Bresolin, F., et al. 2013, *ApJL*, 763, L28, doi: [10.1088/2041-8205/763/2/L28](https://doi.org/10.1088/2041-8205/763/2/L28)
- Chen, Y., Drout, M. R., Piro, A. L., et al. 2023, *ApJ*, 955, 42, doi: [10.3847/1538-4357/ace965](https://doi.org/10.3847/1538-4357/ace965)
- Chini, R., Hoffmeister, V. H., Nasserri, A., Stahl, O., & Zinnecker, H. 2012, *MNRAS*, 424, 1925, doi: [10.1111/j.1365-2966.2012.21317.x](https://doi.org/10.1111/j.1365-2966.2012.21317.x)
- Chrimes, A. A., Coppejans, D. L., Jonker, P. G., et al. 2024a, *A&A*, 691, A329, doi: [10.1051/0004-6361/202451172](https://doi.org/10.1051/0004-6361/202451172)
- Chrimes, A. A., Jonker, P. G., Levan, A. J., et al. 2024b, *MNRAS*, 527, L47, doi: [10.1093/mnras/sl4145](https://doi.org/10.1093/mnras/sl4145)

- Cid Fernandes, R., Stasińska, G., Schlickmann, M. S., et al. 2010, *MNRAS*, 403, 1036, doi: [10.1111/j.1365-2966.2009.16185.x](https://doi.org/10.1111/j.1365-2966.2009.16185.x)
- Conroy, C., & Gunn, J. E. 2010, *ApJ*, 712, 833, doi: [10.1088/0004-637X/712/2/833](https://doi.org/10.1088/0004-637X/712/2/833)
- Conroy, C., Gunn, J. E., & White, M. 2009, *ApJ*, 699, 486, doi: [10.1088/0004-637X/699/1/486](https://doi.org/10.1088/0004-637X/699/1/486)
- Coppejans, D. L., Margutti, R., Terreran, G., et al. 2020, *ApJL*, 895, L23, doi: [10.3847/2041-8213/ab8cc7](https://doi.org/10.3847/2041-8213/ab8cc7)
- Dey, A., Schlegel, D. J., Lang, D., et al. 2019, *AJ*, 157, 168, doi: [10.3847/1538-3881/ab089d](https://doi.org/10.3847/1538-3881/ab089d)
- Dong, Y., Villar, V. A., Nugent, A., et al. 2025, arXiv e-prints, arXiv:2511.03926, doi: [10.48550/arXiv.2511.03926](https://doi.org/10.48550/arXiv.2511.03926)
- Draine, B. T., & Li, A. 2007, *ApJ*, 657, 810, doi: [10.1086/511055](https://doi.org/10.1086/511055)
- Drout, M. R., Chornock, R., Soderberg, A. M., et al. 2014, *ApJ*, 794, 23, doi: [10.1088/0004-637X/794/1/23](https://doi.org/10.1088/0004-637X/794/1/23)
- Dunstall, P. R., Dufton, P. L., Sana, H., et al. 2015, *A&A*, 580, A93, doi: [10.1051/0004-6361/201526192](https://doi.org/10.1051/0004-6361/201526192)
- Falcón-Barroso, J., Sánchez-Blázquez, P., Vazdekis, A., et al. 2011, *A&A*, 532, A95, doi: [10.1051/0004-6361/201116842](https://doi.org/10.1051/0004-6361/201116842)
- Fong, W.-f., Nugent, A. E., Dong, Y., et al. 2022, *ApJ*, 940, 56, doi: [10.3847/1538-4357/ac91d0](https://doi.org/10.3847/1538-4357/ac91d0)
- Fruchter, A. S., Levan, A. J., Strolger, L., et al. 2006, *Nature*, 441, 463, doi: [10.1038/nature04787](https://doi.org/10.1038/nature04787)
- Fryer, C. L., Burns, E., Ho, A. Y. Q., et al. 2025, *ApJ*, 986, 185, doi: [10.3847/1538-4357/add474](https://doi.org/10.3847/1538-4357/add474)
- Fryer, C. L., & Woosley, S. E. 1998, *ApJL*, 502, L9, doi: [10.1086/311493](https://doi.org/10.1086/311493)
- Fryer, C. L., Woosley, S. E., & Hartmann, D. H. 1999, *ApJ*, 526, 152, doi: [10.1086/307992](https://doi.org/10.1086/307992)
- Galbany, L., Anderson, J. P., Rosales-Ortega, F. F., et al. 2016, *MNRAS*, 455, 4087, doi: [10.1093/mnras/stv2620](https://doi.org/10.1093/mnras/stv2620)
- Gallazzi, A., Charlot, S., Brinchmann, J., White, S. D. M., & Tremonti, C. A. 2005, *MNRAS*, 362, 41, doi: [10.1111/j.1365-2966.2005.09321.x](https://doi.org/10.1111/j.1365-2966.2005.09321.x)
- Gaspari, N., Stevance, H. F., Levan, A. J., Chrimes, A. A., & Lyman, J. D. 2024, *A&A*, 692, A21, doi: [10.1051/0004-6361/202450908](https://doi.org/10.1051/0004-6361/202450908)
- Goldstein, A., Veres, P., Burns, E., et al. 2017, *ApJL*, 848, L14, doi: [10.3847/2041-8213/aa8f41](https://doi.org/10.3847/2041-8213/aa8f41)
- Govreen-Segal, T., Nakar, E., Hotokezaka, K., Irwin, C. M., & Quataert, E. 2026, arXiv e-prints, arXiv:2601.18887, doi: [10.48550/arXiv.2601.18887](https://doi.org/10.48550/arXiv.2601.18887)
- Greene, J. E., Lancaster, L., Ting, Y.-S., et al. 2021, *ApJ*, 917, 17, doi: [10.3847/1538-4357/ac0896](https://doi.org/10.3847/1538-4357/ac0896)
- Guolo, M. 2026, arXiv e-prints, arXiv:2602.12970, doi: [10.48550/arXiv.2602.12970](https://doi.org/10.48550/arXiv.2602.12970)
- Guolo, M., Mummery, A., van Velzen, S., et al. 2026, arXiv e-prints, arXiv:2602.12272, doi: [10.48550/arXiv.2602.12272](https://doi.org/10.48550/arXiv.2602.12272)
- Gutiérrez, C. P., Mattila, S., Lundqvist, P., et al. 2024, *ApJ*, 977, 162, doi: [10.3847/1538-4357/ad89a5](https://doi.org/10.3847/1538-4357/ad89a5)
- Heger, A., Fryer, C. L., Woosley, S. E., Langer, N., & Hartmann, D. H. 2003, *ApJ*, 591, 288, doi: [10.1086/375341](https://doi.org/10.1086/375341)
- Hinshaw, G., Larson, D., Komatsu, E., et al. 2013, *ApJS*, 208, 19, doi: [10.1088/0067-0049/208/2/19](https://doi.org/10.1088/0067-0049/208/2/19)
- Ho, A. Y. Q., Phinney, E. S., Ravi, V., et al. 2019, *ApJ*, 871, 73, doi: [10.3847/1538-4357/aaf473](https://doi.org/10.3847/1538-4357/aaf473)
- Ho, A. Y. Q., Perley, D. A., Kulkarni, S. R., et al. 2020, *ApJ*, 895, 49, doi: [10.3847/1538-4357/ab8bcf](https://doi.org/10.3847/1538-4357/ab8bcf)
- Ho, A. Y. Q., Margalit, B., Bremer, M., et al. 2022, *ApJ*, 932, 116, doi: [10.3847/1538-4357/ac4e97](https://doi.org/10.3847/1538-4357/ac4e97)
- Ho, A. Y. Q., Perley, D. A., Chen, P., et al. 2023a, *Nature*, 623, 927, doi: [10.1038/s41586-023-06673-6](https://doi.org/10.1038/s41586-023-06673-6)
- Ho, A. Y. Q., Perley, D. A., Gal-Yam, A., et al. 2023b, *ApJ*, 949, 120, doi: [10.3847/1538-4357/acc533](https://doi.org/10.3847/1538-4357/acc533)
- Horowicz, A., & Margalit, B. 2026, *ApJ*, 996, 78, doi: [10.3847/1538-4357/ae1f11](https://doi.org/10.3847/1538-4357/ae1f11)
- Hosseinzadeh, G., McCully, C., Zabludoff, A. I., et al. 2019, *ApJL*, 871, L9, doi: [10.3847/2041-8213/aafc61](https://doi.org/10.3847/2041-8213/aafc61)
- Hsu, B., Blanchard, P. K., Berger, E., & Gomez, S. 2024, *ApJ*, 961, 169, doi: [10.3847/1538-4357/ad12be](https://doi.org/10.3847/1538-4357/ad12be)
- Hu, M., Yan, S., Wang, X., et al. 2026, arXiv e-prints, arXiv:2601.01333, doi: [10.48550/arXiv.2601.01333](https://doi.org/10.48550/arXiv.2601.01333)
- Inkenhaag, A., Levan, A. J., Mummery, A., & Jonker, P. G. 2025, *MNRAS*, 544, L108, doi: [10.1093/mnras/slaf107](https://doi.org/10.1093/mnras/slaf107)
- Ivezić, Ž., Kahn, S. M., Tyson, J. A., et al. 2019, *ApJ*, 873, 111, doi: [10.3847/1538-4357/ab042c](https://doi.org/10.3847/1538-4357/ab042c)
- Johnson, B. D., Leja, J., Conroy, C., & Speagle, J. S. 2021, *ApJS*, 254, 22, doi: [10.3847/1538-4365/abef67](https://doi.org/10.3847/1538-4365/abef67)
- Jones, D. O., McGill, P., Manning, T. A., et al. 2024, arXiv e-prints, arXiv:2410.17322, doi: [10.48550/arXiv.2410.17322](https://doi.org/10.48550/arXiv.2410.17322)
- Kaasinen, M., Kewley, L., Bian, F., et al. 2018, *MNRAS*, 477, 5568, doi: [10.1093/mnras/sty1012](https://doi.org/10.1093/mnras/sty1012)
- Kasen, D., & Bildsten, L. 2010, *ApJ*, 717, 245, doi: [10.1088/0004-637X/717/1/245](https://doi.org/10.1088/0004-637X/717/1/245)
- Kauffmann, G., Heckman, T. M., Tremonti, C., et al. 2003, *MNRAS*, 346, 1055, doi: [10.1111/j.1365-2966.2003.07154.x](https://doi.org/10.1111/j.1365-2966.2003.07154.x)
- Kelly, P. L., & Kirshner, R. P. 2012, *ApJ*, 759, 107, doi: [10.1088/0004-637X/759/2/107](https://doi.org/10.1088/0004-637X/759/2/107)
- Kelly, P. L., Kirshner, R. P., & Pahre, M. 2008, *ApJ*, 687, 1201, doi: [10.1086/591925](https://doi.org/10.1086/591925)
- Kewley, L. J., & Dopita, M. A. 2002, *ApJS*, 142, 35, doi: [10.1086/341326](https://doi.org/10.1086/341326)

- Kewley, L. J., Dopita, M. A., Sutherland, R. S., Heisler, C. A., & Trevena, J. 2001, *ApJ*, 556, 121, doi: [10.1086/321545](https://doi.org/10.1086/321545)
- Kewley, L. J., Groves, B., Kauffmann, G., & Heckman, T. 2006, *MNRAS*, 372, 961, doi: [10.1111/j.1365-2966.2006.10859.x](https://doi.org/10.1111/j.1365-2966.2006.10859.x)
- Kewley, L. J., Maier, C., Yabe, K., et al. 2013, *ApJL*, 774, L10, doi: [10.1088/2041-8205/774/1/L10](https://doi.org/10.1088/2041-8205/774/1/L10)
- Kewley, L. J., Nicholls, D. C., & Sutherland, R. S. 2019, *ARA&A*, 57, 511, doi: [10.1146/annurev-astro-081817-051832](https://doi.org/10.1146/annurev-astro-081817-051832)
- Khatami, D. K., & Kasen, D. N. 2024, *ApJ*, 972, 140, doi: [10.3847/1538-4357/ad60c0](https://doi.org/10.3847/1538-4357/ad60c0)
- Klencki, J., & Metzger, B. D. 2025, arXiv e-prints, arXiv:2510.09745, doi: [10.48550/arXiv.2510.09745](https://doi.org/10.48550/arXiv.2510.09745)
- Klencki, J., Nelemans, G., Istrate, A. G., & Pols, O. 2020, *A&A*, 638, A55, doi: [10.1051/0004-6361/202037694](https://doi.org/10.1051/0004-6361/202037694)
- Kriek, M., & Conroy, C. 2013, *ApJL*, 775, L16, doi: [10.1088/2041-8205/775/1/L16](https://doi.org/10.1088/2041-8205/775/1/L16)
- Kuin, N. P. M., Wu, K., Oates, S., et al. 2019, *MNRAS*, 487, 2505, doi: [10.1093/mnras/stz053](https://doi.org/10.1093/mnras/stz053)
- Laigle, C., McCracken, H. J., Ilbert, O., et al. 2016, *ApJS*, 224, 24, doi: [10.3847/0067-0049/224/2/24](https://doi.org/10.3847/0067-0049/224/2/24)
- Lang, D., Hogg, D. W., Mierle, K., Blanton, M., & Roweis, S. 2010, *AJ*, 139, 1782, doi: [10.1088/0004-6256/139/5/1782](https://doi.org/10.1088/0004-6256/139/5/1782)
- LeBaron, N., Margutti, R., Chornock, R., et al. 2026, *ApJL*, 997, L10, doi: [10.3847/2041-8213/ae2910](https://doi.org/10.3847/2041-8213/ae2910)
- Leja, J., Johnson, B. D., Conroy, C., et al. 2019, *ApJ*, 877, 140, doi: [10.3847/1538-4357/ab1d5a](https://doi.org/10.3847/1538-4357/ab1d5a)
- Leja, J., Speagle, J. S., Ting, Y.-S., et al. 2022, *ApJ*, 936, 165, doi: [10.3847/1538-4357/ac887d](https://doi.org/10.3847/1538-4357/ac887d)
- Leloudas, G., Schulze, S., Krühler, T., et al. 2015, *MNRAS*, 449, 917, doi: [10.1093/mnras/stv320](https://doi.org/10.1093/mnras/stv320)
- Leung, S.-C., Blinnikov, S., Nomoto, K., et al. 2020, *ApJ*, 903, 66, doi: [10.3847/1538-4357/abba33](https://doi.org/10.3847/1538-4357/abba33)
- Li, W., Chornock, R., Leaman, J., et al. 2011, *MNRAS*, 412, 1473, doi: [10.1111/j.1365-2966.2011.18162.x](https://doi.org/10.1111/j.1365-2966.2011.18162.x)
- Lovegrove, E., Woosley, S. E., & Zhang, W. 2017, *ApJ*, 845, 103, doi: [10.3847/1538-4357/aa7b7d](https://doi.org/10.3847/1538-4357/aa7b7d)
- LSST Science Collaboration, Abell, P. A., Allison, J., et al. 2009, arXiv e-prints, arXiv:0912.0201, doi: [10.48550/arXiv.0912.0201](https://doi.org/10.48550/arXiv.0912.0201)
- Lunnan, R., Chornock, R., Berger, E., et al. 2014, *ApJ*, 787, 138, doi: [10.1088/0004-637X/787/2/138](https://doi.org/10.1088/0004-637X/787/2/138)
- . 2015, *ApJ*, 804, 90, doi: [10.1088/0004-637X/804/2/90](https://doi.org/10.1088/0004-637X/804/2/90)
- Mandhai, S., Lamb, G. P., Tanvir, N. R., et al. 2022, *MNRAS*, 514, 2716, doi: [10.1093/mnras/stac1473](https://doi.org/10.1093/mnras/stac1473)
- Maoz, D., Mannucci, F., & Nelemans, G. 2014, *ARA&A*, 52, 107, doi: [10.1146/annurev-astro-082812-141031](https://doi.org/10.1146/annurev-astro-082812-141031)
- Margalit, B., Quataert, E., & Ho, A. Y. Q. 2022, *ApJ*, 928, 122, doi: [10.3847/1538-4357/ac53b0](https://doi.org/10.3847/1538-4357/ac53b0)
- Margutti, R., Metzger, B. D., Chornock, R., et al. 2019, *ApJ*, 872, 18, doi: [10.3847/1538-4357/aafa01](https://doi.org/10.3847/1538-4357/aafa01)
- Metzger, B. D. 2022, *ApJ*, 932, 84, doi: [10.3847/1538-4357/ac6d59](https://doi.org/10.3847/1538-4357/ac6d59)
- Metzger, B. D., Margalit, B., Kasen, D., & Quataert, E. 2015, *MNRAS*, 454, 3311, doi: [10.1093/mnras/stv2224](https://doi.org/10.1093/mnras/stv2224)
- Migliori, G., Margutti, R., Metzger, B. D., et al. 2024, *ApJL*, 963, L24, doi: [10.3847/2041-8213/ad2764](https://doi.org/10.3847/2041-8213/ad2764)
- Modjaz, M., Kewley, L., Bloom, J. S., et al. 2011, *ApJL*, 731, L4, doi: [10.1088/2041-8205/731/1/L4](https://doi.org/10.1088/2041-8205/731/1/L4)
- Moe, M., & Di Stefano, R. 2017, *ApJS*, 230, 15, doi: [10.3847/1538-4365/aa6fb6](https://doi.org/10.3847/1538-4365/aa6fb6)
- Nakajima, K., & Ouchi, M. 2014, *MNRAS*, 442, 900, doi: [10.1093/mnras/stu902](https://doi.org/10.1093/mnras/stu902)
- Nayana, A. J., Margutti, R., Wiston, E., et al. 2025, *ApJL*, 993, L6, doi: [10.3847/2041-8213/ae0b4d](https://doi.org/10.3847/2041-8213/ae0b4d)
- Neights, E., Burns, E., Fryer, C. L., et al. 2026, *MNRAS*, 545, staf2019, doi: [10.1093/mnras/staf2019](https://doi.org/10.1093/mnras/staf2019)
- Nicholl, M., Guillochon, J., & Berger, E. 2017, *ApJ*, 850, 55, doi: [10.3847/1538-4357/aa9334](https://doi.org/10.3847/1538-4357/aa9334)
- Nicholl, M., Smartt, S. J., Jerkstrand, A., et al. 2015, *MNRAS*, 452, 3869, doi: [10.1093/mnras/stv1522](https://doi.org/10.1093/mnras/stv1522)
- Niino, Y., Aoki, K., Hashimoto, T., et al. 2017, *PASJ*, 69, 27, doi: [10.1093/pasj/psw133](https://doi.org/10.1093/pasj/psw133)
- Nugent, A. E., Villar, V. A., Gagliano, A., et al. 2026, *ApJ*, 997, 38, doi: [10.3847/1538-4357/ae247b](https://doi.org/10.3847/1538-4357/ae247b)
- Omand, C. M. B., Sarin, N., Lamb, G. P., et al. 2026, arXiv e-prints, arXiv:2601.03372, doi: [10.48550/arXiv.2601.03372](https://doi.org/10.48550/arXiv.2601.03372)
- Pan, K.-C., Ruiz-Lapuente, P., & González Hernández, J. I. 2026, *ApJ*, 996, 35, doi: [10.3847/1538-4357/ae1b9e](https://doi.org/10.3847/1538-4357/ae1b9e)
- Paterson, K. 2021
- Paxton, B., Schwab, J., Bauer, E. B., et al. 2018, *ApJS*, 234, 34, doi: [10.3847/1538-4365/aaa5a8](https://doi.org/10.3847/1538-4365/aaa5a8)
- Pellegrino, C., Howell, D. A., Vinkó, J., et al. 2022, *ApJ*, 926, 125, doi: [10.3847/1538-4357/ac3e63](https://doi.org/10.3847/1538-4357/ac3e63)
- Perley, D. A., & Perley, R. A. 2013, *ApJ*, 778, 172, doi: [10.1088/0004-637X/778/2/172](https://doi.org/10.1088/0004-637X/778/2/172)
- Perley, D. A., Quimby, R. M., Yan, L., et al. 2016, *ApJ*, 830, 13, doi: [10.3847/0004-637X/830/1/13](https://doi.org/10.3847/0004-637X/830/1/13)
- Perley, D. A., Mazzali, P. A., Yan, L., et al. 2019, *MNRAS*, 484, 1031, doi: [10.1093/mnras/sty3420](https://doi.org/10.1093/mnras/sty3420)
- Perley, D. A., Ho, A. Y. Q., Yao, Y., et al. 2021, *MNRAS*, 508, 5138, doi: [10.1093/mnras/stab2785](https://doi.org/10.1093/mnras/stab2785)
- Perley, D. A., Ho, A. Y. Q., McGrath, Z., et al. 2026, arXiv e-prints, arXiv:2601.03337, doi: [10.48550/arXiv.2601.03337](https://doi.org/10.48550/arXiv.2601.03337)

- Prentice, S. J., Maguire, K., Smartt, S. J., et al. 2018, *ApJL*, 865, L3, doi: [10.3847/2041-8213/aadd90](https://doi.org/10.3847/2041-8213/aadd90)
- Prieto, J. L., Stanek, K. Z., & Beacom, J. F. 2008, *ApJ*, 673, 999, doi: [10.1086/524654](https://doi.org/10.1086/524654)
- Prochaska, J., Hennawi, J., Westfall, K., et al. 2020, *The Journal of Open Source Software*, 5, 2308, doi: [10.21105/joss.02308](https://doi.org/10.21105/joss.02308)
- Pursiainen, M., Killestein, T. L., Kuncarayakti, H., et al. 2025, *MNRAS*, 537, 3298, doi: [10.1093/mnras/staf232](https://doi.org/10.1093/mnras/staf232)
- Qin, Y.-J., & Zabludoff, A. 2024, *MNRAS*, 533, 3517, doi: [10.1093/mnras/stae1921](https://doi.org/10.1093/mnras/stae1921)
- Quataert, E., Lecoanet, D., & Coughlin, E. R. 2019, *MNRAS*, 485, L83, doi: [10.1093/mnrasl/slz031](https://doi.org/10.1093/mnrasl/slz031)
- Renzo, M., Zapartas, E., de Mink, S. E., et al. 2019, *A&A*, 624, A66, doi: [10.1051/0004-6361/201833297](https://doi.org/10.1051/0004-6361/201833297)
- Ricarte, A., Tremmel, M., Natarajan, P., & Quinn, T. 2021, *ApJL*, 916, L18, doi: [10.3847/2041-8213/ac1170](https://doi.org/10.3847/2041-8213/ac1170)
- Sana, H., de Mink, S. E., de Koter, A., et al. 2012, *Science*, 337, 444, doi: [10.1126/science.1223344](https://doi.org/10.1126/science.1223344)
- Schlafly, E. F., & Finkbeiner, D. P. 2011, *ApJ*, 737, 103, doi: [10.1088/0004-637X/737/2/103](https://doi.org/10.1088/0004-637X/737/2/103)
- Schulze, S., Krühler, T., Leloudas, G., et al. 2018, *MNRAS*, 473, 1258, doi: [10.1093/mnras/stx2352](https://doi.org/10.1093/mnras/stx2352)
- Schulze, S., Yaron, O., Sollerman, J., et al. 2021, *ApJS*, 255, 29, doi: [10.3847/1538-4365/abff5e](https://doi.org/10.3847/1538-4365/abff5e)
- Sevilla, C., Ho, A. Y. Q., J., N. A., et al. 2026, arXiv e-prints, arXiv:2601.18926. <https://arxiv.org/abs/2601.18926>
- Shi, J., Auchettl, K., Hoogendam, W. B., et al. 2026, arXiv e-prints, arXiv:2602.16227, doi: [10.48550/arXiv.2602.16227](https://doi.org/10.48550/arXiv.2602.16227)
- Skelton, R. E., Whitaker, K. E., Momcheva, I. G., et al. 2014, *ApJS*, 214, 24, doi: [10.1088/0067-0049/214/2/24](https://doi.org/10.1088/0067-0049/214/2/24)
- Skrutskie, M. F., Cutri, R. M., Stiening, R., et al. 2006, *AJ*, 131, 1163, doi: [10.1086/498708](https://doi.org/10.1086/498708)
- Smartt, S. J. 2015, *PASA*, 32, e016, doi: [10.1017/pasa.2015.17](https://doi.org/10.1017/pasa.2015.17)
- Smartt, S. J., Eldridge, J. J., Crockett, R. M., & Maund, J. R. 2009, *MNRAS*, 395, 1409, doi: [10.1111/j.1365-2966.2009.14506.x](https://doi.org/10.1111/j.1365-2966.2009.14506.x)
- Smith, N. 2014, *ARA&A*, 52, 487, doi: [10.1146/annurev-astro-081913-040025](https://doi.org/10.1146/annurev-astro-081913-040025)
- Smith, N., Li, W., Filippenko, A. V., & Chornock, R. 2011, *MNRAS*, 412, 1522, doi: [10.1111/j.1365-2966.2011.17229.x](https://doi.org/10.1111/j.1365-2966.2011.17229.x)
- Speagle, J. S. 2020, *MNRAS*, 493, 3132, doi: [10.1093/mnras/staa278](https://doi.org/10.1093/mnras/staa278)
- Speagle, J. S., Steinhardt, C. L., Capak, P. L., & Silverman, J. D. 2014, *ApJS*, 214, 15, doi: [10.1088/0067-0049/214/2/15](https://doi.org/10.1088/0067-0049/214/2/15)
- Stein, R., Carney, J., Ward, C., et al. 2026, arXiv e-prints, arXiv:2602.10180, doi: [10.48550/arXiv.2602.10180](https://doi.org/10.48550/arXiv.2602.10180)
- Sun, N.-C., Maund, J. R., Shao, Y., & Janiak, I. A. 2023, *MNRAS*, 519, 3785, doi: [10.1093/mnras/stac3773](https://doi.org/10.1093/mnras/stac3773)
- Svensson, K. M., Levan, A. J., Tanvir, N. R., Fruchter, A. S., & Strolger, L.-G. 2010, *MNRAS*, 405, 57, doi: [10.1111/j.1365-2966.2010.16442.x](https://doi.org/10.1111/j.1365-2966.2010.16442.x)
- Tacchella, S., Conroy, C., Faber, S. M., et al. 2022, *ApJ*, 926, 134, doi: [10.3847/1538-4357/ac449b](https://doi.org/10.3847/1538-4357/ac449b)
- Taggart, K., & Perley, D. A. 2021, *MNRAS*, 503, 3931, doi: [10.1093/mnras/stab174](https://doi.org/10.1093/mnras/stab174)
- Thöne, C. C., de Ugarte Postigo, A., Fryer, C. L., et al. 2011, *Nature*, 480, 72, doi: [10.1038/nature10611](https://doi.org/10.1038/nature10611)
- Tremonti, C. A., Heckman, T. M., Kauffmann, G., et al. 2004, *ApJ*, 613, 898, doi: [10.1086/423264](https://doi.org/10.1086/423264)
- Tsuna, D., & Lu, W. 2025, *ApJ*, 986, 84, doi: [10.3847/1538-4357/add158](https://doi.org/10.3847/1538-4357/add158)
- Veilleux, S., & Osterbrock, D. E. 1987, *ApJS*, 63, 295, doi: [10.1086/191166](https://doi.org/10.1086/191166)
- Vurm, I., & Metzger, B. D. 2021, *ApJ*, 917, 77, doi: [10.3847/1538-4357/ac0826](https://doi.org/10.3847/1538-4357/ac0826)
- Wagg, T., Dalcanton, J. J., Renzo, M., et al. 2025, *AJ*, 170, 192, doi: [10.3847/1538-3881/adf55e](https://doi.org/10.3847/1538-3881/adf55e)
- Wang, F. Y., & Dai, Z. G. 2014, *ApJS*, 213, 15, doi: [10.1088/0067-0049/213/1/15](https://doi.org/10.1088/0067-0049/213/1/15)
- Wang, X., Wang, L., Filippenko, A. V., Zhang, T., & Zhao, X. 2013, *Science*, 340, 170, doi: [10.1126/science.1231502](https://doi.org/10.1126/science.1231502)
- Whitaker, K. E., Franx, M., Leja, J., et al. 2014, *ApJ*, 795, 104, doi: [10.1088/0004-637X/795/2/104](https://doi.org/10.1088/0004-637X/795/2/104)
- Winter-Granic, M., & Quataert, E. 2025, arXiv e-prints, arXiv:2512.09017, doi: [10.48550/arXiv.2512.09017](https://doi.org/10.48550/arXiv.2512.09017)
- Woosley, S. E. 1993, *ApJ*, 405, 273, doi: [10.1086/172359](https://doi.org/10.1086/172359)
- . 2017, *ApJ*, 836, 244, doi: [10.3847/1538-4357/836/2/244](https://doi.org/10.3847/1538-4357/836/2/244)
- Woosley, S. E., & Bloom, J. S. 2006, *ARA&A*, 44, 507, doi: [10.1146/annurev.astro.43.072103.150558](https://doi.org/10.1146/annurev.astro.43.072103.150558)
- Wright, E. L., Eisenhardt, P. R. M., Mainzer, A. K., et al. 2010, *AJ*, 140, 1868, doi: [10.1088/0004-6256/140/6/1868](https://doi.org/10.1088/0004-6256/140/6/1868)
- Yao, Y., Ho, A. Y. Q., Medvedev, P., et al. 2022, *ApJ*, 934, 104, doi: [10.3847/1538-4357/ac7a41](https://doi.org/10.3847/1538-4357/ac7a41)
- Zevin, M., Kelley, L. Z., Nugent, A., et al. 2020, *ApJ*, 904, 190, doi: [10.3847/1538-4357/abc266](https://doi.org/10.3847/1538-4357/abc266)
- Zhang, W., & Fryer, C. L. 2001, *ApJ*, 550, 357, doi: [10.1086/319734](https://doi.org/10.1086/319734)

## APPENDIX

## A. HOST GALAXY OBSERVATIONS

Here, we highlight LFBOT host galaxy photometric (Table A1) and spectroscopic (Table A2) observations.

**Table A1.** Host Galaxy Photometry

LFBOT	Host R.A.	Host Decl.	Instrument or Survey	Filter	AB Mag	Ref.
AT2018cow	16 <sup>h</sup> 16 <sup>m</sup> 00.58 <sup>s</sup>	+22 <sup>d</sup> 16 <sup>m</sup> 08.300 <sup>s</sup>	GALEX	FUV	18.38 ± 0.21	Perley et al. (2019)
			GALEX	NUV	17.88 ± 0.04	Perley et al. (2019)
			SDSS	<i>u</i>	16.76 ± 0.04	Perley et al. (2019)
			SDSS	<i>g</i>	15.58 ± 0.003	Perley et al. (2019)
			SDSS	<i>r</i>	15.02 ± 0.002	Perley et al. (2019)
			SDSS	<i>i</i>	14.73 ± 0.01	Perley et al. (2019)
			SDSS	<i>z</i>	14.53 ± 0.02	Perley et al. (2019)
			Pan-STARRS	<i>y</i>	14.48 ± 0.05	Perley et al. (2019)
			2MASS	<i>J</i>	14.15 ± 0.05	Perley et al. (2019)
			2MASS	<i>H</i>	14.07 ± 0.08	Perley et al. (2019)
			2MASS	<i>K</i>	14.32 ± 0.11	Perley et al. (2019)
			WISE	<i>w1</i>	15.37 ± 0.01	Perley et al. (2019)
			WISE	<i>w2</i>	16.01 ± 0.02	Perley et al. (2019)
			WISE	<i>w3</i>	14.99 ± 0.03	Perley et al. (2019)
			WISE	<i>w4</i>	14.67 ± 0.24	Perley et al. (2019)
CSS161010	04 <sup>h</sup> 48 <sup>m</sup> 34.398 <sup>s</sup>	-08 <sup>d</sup> 18 <sup>m</sup> 04.337 <sup>s</sup>	Pan-STARRS	<i>g</i>	21.35 ± 0.08	This work
			Pan-STARRS	<i>r</i>	21.99 ± 0.10	This work
			Pan-STARRS	<i>i</i>	21.00 ± 0.05	This work
			Pan-STARRS	<i>z</i>	20.36 ± 0.10	This work
			Pan-STARRS	<i>y</i>	20.22 ± 0.30	This work
ZTF18abvkw1	02 <sup>h</sup> 00 <sup>m</sup> 15.238 <sup>s</sup>	+16 <sup>d</sup> 47 <sup>m</sup> 57.151 <sup>s</sup>	SDSS	<i>u</i>	21.95 ± 0.20	Ho et al. (2020)
			Pan-STARRS	<i>g</i>	21.33 ± 0.07	This work
			Pan-STARRS	<i>r</i>	21.09 ± 0.05	This work
			Pan-STARRS	<i>i</i>	21.03 ± 0.05	This work
			Pan-STARRS	<i>z</i>	20.27 ± 0.07	This work
			Pan-STARRS	<i>y</i>	19.87 ± 0.15	This work
			2MASS	<i>J</i>	18.88 ± 0.04	This work
			2MASS	<i>K</i>	17.70 ± 0.04	This work
AT2020mrf	15 <sup>h</sup> 47 <sup>m</sup> 54.20 <sup>s</sup>	+44 <sup>d</sup> 39 <sup>m</sup> 07.01 <sup>s</sup>	GALEX	FUV	> 23.28	Yao et al. (2022)
			GALEX	NUV	> 23.56	Yao et al. (2022)
			HSC	<i>g</i>	23.28 ± 0.03	Yao et al. (2022)
			HSC	<i>r</i>	23.15 ± 0.05	Yao et al. (2022)
			HSC	<i>i</i>	22.64 ± 0.04	Yao et al. (2022)
			HSC	<i>z</i>	22.72 ± 0.08	Yao et al. (2022)
			HSC	<i>y</i>	22.36 ± 0.13	Yao et al. (2022)
AT2020xnd	22 <sup>h</sup> 20 <sup>m</sup> 02.04 <sup>s</sup>	-2 <sup>d</sup> 50 <sup>m</sup> 25.44 <sup>s</sup>	VLT/FORS2	<i>u</i>	25.6 ± 0.3	Perley et al. (2021)
			VLT/FORS2	<i>g</i>	24.75 ± 0.10	Perley et al. (2021)
			MMT/Binospec	<i>r</i>	24.03 ± 0.11	This work

**Table A1** *continued*

**Table A1** (*continued*)

LFBOT	Host R.A.	Host Decl.	Instrument or Survey	Filter	AB Mag	Ref.
			VLT/FORS2	<i>I</i>	$24.56 \pm 0.25$	Perley et al. (2021)
AT2022tsd	$03^{\text{h}}20^{\text{m}}10.80^{\text{s}}$	$+8^{\text{d}}44^{\text{m}}57.15^{\text{s}}$	Keck/LRIS	<i>G</i>	$21.41 \pm 0.02$	This work
			MMT/Binospec	<i>r</i>	$20.61 \pm 0.01$	This work
			Pan-STARRS	<i>i</i>	$20.61 \pm 0.06$	This work
			MMT/Binospec	<i>z</i>	$20.13 \pm 0.01$	This work
AT2023fhn	$10^{\text{h}}08^{\text{m}}03.744^{\text{s}}$	$+21^{\text{d}}04^{\text{m}}22.44^{\text{s}}$	SDSS	<i>u</i>	$20.44 \pm 0.01$	This work
			DECaLS	<i>g</i>	$19.46 \pm 0.01$	This work
			Keck/LRIS	<i>V</i>	$19.36 \pm 0.002$	This work
			DECaLS	<i>r</i>	$18.91 \pm 0.01$	This work
			DECaLS	<i>i</i>	$18.60 \pm 0.01$	This work
			DECaLS	<i>z</i>	$18.54 \pm 0.01$	This work
AT2023hkw	$10^{\text{h}}42^{\text{m}}17.64^{\text{s}}$	$+52^{\text{d}}29^{\text{m}}16.32^{\text{s}}$	GALEX	<i>NUV</i>	$>21.44$	This work
			Pan-STARRS	<i>g</i>	$20.82 \pm 0.09$	This work
			Pan-STARRS	<i>r</i>	$19.74 \pm 0.03$	This work
			Pan-STARRS	<i>i</i>	$19.47 \pm 0.02$	This work
			Pan-STARRS	<i>z</i>	$19.23 \pm 0.04$	This work
			Pan-STARRS	<i>y</i>	$19.11 \pm 0.09$	This work
			2MASS	<i>J</i>	$18.09 \pm 0.03$	This work
			2MASS	<i>H</i>	$17.49 \pm 0.02$	This work
AT2023vth	$17^{\text{h}}56^{\text{m}}34.50^{\text{s}}$	$+08^{\text{d}}02^{\text{m}}35.04^{\text{s}}$	GALEX	<i>NUV</i>	$21.19 \pm 0.23$	This work
			Pan-STARRS	<i>g</i>	$19.60 \pm 0.02$	This work
			Pan-STARRS	<i>r</i>	$18.94 \pm 0.01$	This work
			Pan-STARRS	<i>i</i>	$18.56 \pm 0.01$	This work
			Pan-STARRS	<i>z</i>	$18.42 \pm 0.02$	This work
			Pan-STARRS	<i>y</i>	$18.37 \pm 0.04$	This work
			2MASS	<i>J</i>	$17.56 \pm 0.02$	This work
			2MASS	<i>H</i>	$16.64 \pm 0.01$	This work
			2MASS	<i>K</i>	$16.76 \pm 0.01$	This work
AT2024qfm	$23^{\text{h}}21^{\text{m}}23.40^{\text{s}}$	$+11^{\text{d}}56^{\text{m}}32.64^{\text{s}}$	Pan-STARRS	<i>g</i>	$20.58 \pm 0.05$	This work
			Pan-STARRS	<i>r</i>	$19.78 \pm 0.02$	This work
			Pan-STARRS	<i>i</i>	$19.45 \pm 0.02$	This work
			Pan-STARRS	<i>z</i>	$19.21 \pm 0.02$	This work
			MMT/MMIRS	<i>Y</i>	$18.89 \pm 0.02$	This work
			MMT/MMIRS	<i>J</i>	$18.77 \pm 0.01$	This work
			MMT/MMIRS	<i>H</i>	$18.29 \pm 0.03$	This work
			MMT/MMIRS	<i>K</i>	$17.66 \pm 0.03$	This work
AT2024wpp	$02^{\text{h}}42^{\text{m}}05.592^{\text{s}}$	$-16^{\text{d}}57^{\text{m}}26.280^{\text{s}}$	MMT/Binospec	<i>g</i>	$20.19 \pm 0.01$	This work
			Pan-STARRS	<i>r</i>	$19.83 \pm 0.02$	This work
			MMT/Binospec	<i>i</i>	$19.58 \pm 0.02$	This work
			MMT/Binospec	<i>z</i>	$19.34 \pm 0.02$	This work
			MMT/MMIRS	<i>Y</i>	$19.53 \pm 0.04$	This work
			MMT/MMIRS	<i>J</i>	$19.64 \pm 0.04$	This work
			MMT/MMIRS	<i>H</i>	$19.72 \pm 0.06$	This work
			MMT/MMIRS	<i>K</i>	$20.87 \pm 0.12$	This work

NOTE—The localizations and photometric observations for our sample of LFBOT host galaxies. Magnitudes are not corrected for Galactic extinction.

**Table A2.** Host Galaxy Spectroscopy

LFBOT	$z$	Facility/Instrument	Exposures	Lines Identified	Ref.
AT2018cow	0.0141	MMT/Binospec	4×200 s	Ca II H+K, H $\beta$ , [O III] $\lambda$ 5007, Mg $\lambda$ 5175, NaD $\lambda$ 5892, H $\alpha$ , [N II] $\lambda\lambda$ 6549, 6584, [S II] $\lambda\lambda$ 6717, 6731	This work
CSS161010	0.033	Keck/LRIS	3300 s	[O II] $\lambda$ 3727, He I $\lambda$ 3889, Ca II H+K, [O III] $\lambda$ 5007 H $\alpha$ , [N II] $\lambda$ 6584, [S II] $\lambda\lambda$ 6717, 6731	Coppejans et al. (2020)
ZTF18abvkw1*	0.272	Keck/LRIS	1×900 s	[O II] $\lambda$ 3727, He I $\lambda$ 3889, H $\gamma$ , H $\beta$ , H $\gamma$ , [O III] $\lambda\lambda$ 4959, 5007, OI $\lambda$ 6300, H $\alpha$ , [N II] $\lambda\lambda$ 6549, 6584, [S II] $\lambda\lambda$ 6717, 6731	Ho et al. (2020)
AT2020mrf	0.1353	Keck/LRIS	4×850 s	[O II] $\lambda$ 3727, H $\alpha$ , [N II] $\lambda$ 6584	Yao et al. (2022)
AT2020xnd	0.243	MMT/Binospec	4×900 s	None	This work
AT2022tsd	0.256	MMT/Binospec	4×900 s	[O II] $\lambda$ 3727, He I $\lambda$ 3889, H $\gamma$ , H $\beta$ , [O III] $\lambda\lambda$ 4959, 5007, OI $\lambda$ 6300, H $\alpha$ , [N II] $\lambda\lambda$ 6549, 6584, [S II] $\lambda\lambda$ 6717, 6731	This work
AT2023fhn	0.238	MMT/Binospec	6×900 s	[O II] $\lambda$ 3727, Ca II H+K, H $\beta$ , [O III] $\lambda\lambda$ 4959, 5007, OI $\lambda$ 6300, H $\alpha$ , [N II] $\lambda\lambda$ 6549, 6584, [S II] $\lambda\lambda$ 6717, 6731	This work
AT2023hkw	0.335	MMT/Binospec	4×900 s	[O II] $\lambda$ 3727, Ca II H+K, H $\alpha$ , [N II] $\lambda\lambda$ 6549, 6584, [S II] $\lambda\lambda$ 6717, 6731	This work
AT2024qfm	0.227	MMT/Binospec	4×900 s	[O II] $\lambda$ 3727, H $\beta$ , [O III] $\lambda$ 5007, H $\alpha$ , [N II] $\lambda\lambda$ 6549, 6584, [S II] $\lambda\lambda$ 6717, 6731	This work
AT2024wpp	0.0866	MMT/Binospec	3×900 s	[O II] $\lambda$ 3727, Ca II H+K, H $\beta$ , [O III] $\lambda\lambda$ 4959, 5007, OI $\lambda$ 6300, H $\alpha$ , [N II] $\lambda\lambda$ 6549, 6584, [S II] $\lambda\lambda$ 6717, 6731	This work

NOTE—Spectroscopic observations of LFBOT host galaxies. We reduce all available spectroscopic observations, including those that were previously published except for that of ZTF18abvkw1. We also list spectral lines we detect in each of the spectra.

\*Not re-reduced.

## B. HOST GALAXY SED FITS

In Figure B1, we highlight the *Prospector*-produced model SEDs compared to the observed SEDs for each LFBOT host in our sample. For all fits, we find good agreement between the model and observed data.

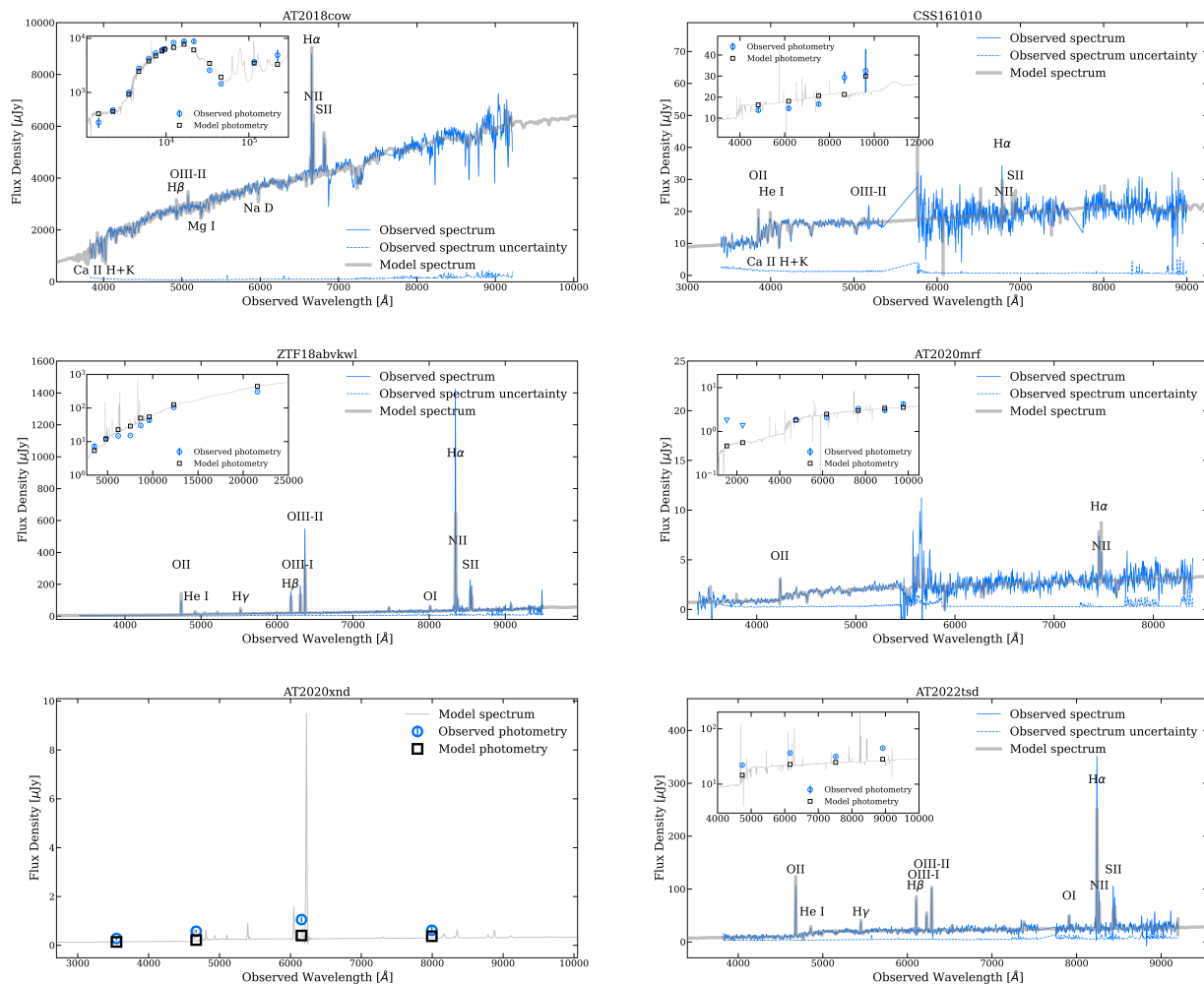


**Figure B1.** The observed photometry (blue circles) and observed spectrum (blue line) compared to the Prospector model photometry (black squares) and spectra (grey lines) for our LFBOT hosts derived at the median of their stellar population property posteriors. We highlight high S/N emission and absorption lines observed in each host spectrum.

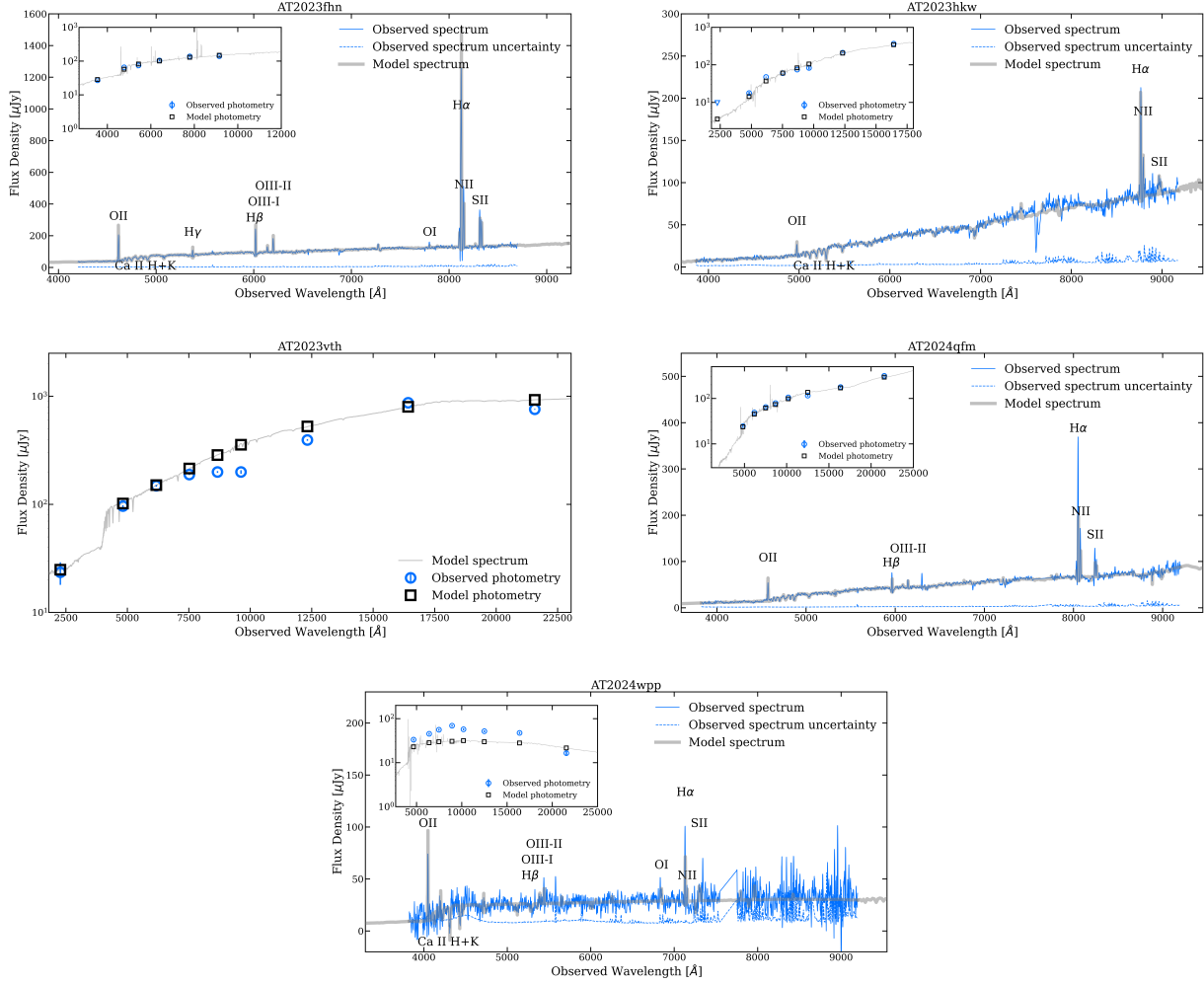


**Figure B1 (Cont.).** The observed photometry (blue circles) and observed spectrum (blue line) compared to the Prospector model photometry (black squares) and spectra (grey lines) for our LFBOT hosts derived at the median of their stellar population property posteriors. We highlight high S/N emission and absorption lines observed in each host spectrum.